Progress in Polymer Science 156 (2024) 101865

Contents lists available at ScienceDirect

Progress in Polymer Science

journal homepage: www.elsevier.com/locate/progpolymsci

Infrared plastic optics and photonic devices using chalcogenide hybrid inorganic/organic polymers via inverse vulcanization of elemental sulfur

Jeffrey Pyun [a,b,*], Robert A. Norwood [b,c]

[a] Department of Chemistry and Biochemistry, University of Arizona, Tucson, AZ 85721, USA
[b] J C Wyant College of Optical Sciences, USA
[c] Department of Materials Science & Engineering, College of Engineering, University of Arizona, Tucson, AZ 85721, USA

ARTICLE INFO

Article history:
Received 7 April 2024
Revised 8 June 2024
Accepted 6 August 2024
Available online 8 August 2024

Keywords:
Inverse vulcanization
Sulfur
Infrared imaging
Integrated photonics
Polymers
Waveguides
Ring resonators

ABSTRACT

Since the invention of inverse vulcanization and high sulfur content polymers, termed *Chalcogenide Hybrid Inorganic/Organic Polymers*, the application of these polymers as optical materials for IR optics & photonics has garnered interest from groups around the world. Earlier publications and review papers have focused on the polymer chemistry aspects of inverse vulcanization, however, recent work in the past decade has seen tremendous new advances in polymer processing, rheology, and optical component (nano-micro) fabrication of lenses and photonic devices across the infrared spectrum. There is an urgent need for a review surveying both new polymer chemistry and polymer engineering aspects of this important new field, for the integration of these new optical polymers into imaging, communications, and sensing systems. In this submission, we review the fabrication and polymer processing of inverse vulcanized organopolysulfides made from elemental sulfur for IR optics and photonics. We survey recent work in the SWIR and MWIR spectrum for the development of integrated photonics devices using high sulfur content polymers, along with the fabrication and testing of LWIR bulk plastic optics using this new class of optical polymers.

1. Introduction

The controllable manipulation of light propagation with a high degree of precision in solid media is integral to the fabrication of various optical devices that function in both the visible and infrared (IR) spectrum. IR photonics has evolved into numerous approaches and systems for imaging, sensing and communication, along with IR spectroscopy for the chemical identification of molecular compounds [1]. IR optical systems span a broad range of wavelengths in the near infrared (NIR, 700–1000 nm) the short wave infrared (SWIR, 1000–3000 nm), the midwave infrared (MWIR, 3 μm-5 μm) and the long wave infrared (LWIR, 7–14 μm) covering numerous integrated 2-D planar on chip devices or sensors, along with free-form optics for use as lenses, diffusers, polarizers and other optical components for IR imaging. Due to the broad spectral window covering the NIR-SWIR-MWIR-LWIR, numerous discrete optical material options are available, which include glass, metal oxides, aluminosilicates, polymeric materials, semiconductors and chalcogenide glass for use as integrated optical or bulk optical elements. For use in the longer MWIR and LWIR spectrum, optical materials with acceptable transparency are limited to heavy atom containing inorganic covalent solids (e.g., sapphire-Al_2O_3, silicon, germanium, chalcogenide glass). These inorganic materials possess high transmission at MWIR and LWIR wavelengths and high refractive indices (n ~2–4), but are expensive to both access as raw materials and for processing to fabricate into optical components [2]. Numerous optical polymer materials for use in photonics and imaging are viable

Abbreviations: SWIR, short wave infrared; MWIR, mid-wave infrared; LWIR, long wave infrared; NIR, near infrared; IR, infrared; PMMA, poly(methyl methacrylate); PC, polycarbonate; RI, refractive index; CHIPs, Chalcogenide Hybrid Inorganic/Organic Polymers; ChG's, chalcogenide glass; S_8, elemental sulfur; Se, selenium; sCVD, sulfur chemical vapor deposition; DIB, 1,3-isopropenylbenzene; Poly(S-*r*-DIB), poly(sulfur-*random*-(1,3-diisopropenylbenzene)); DVB, 1,3- and 1,4-divinylbenzene; Poly(S-*r*-DVB), poly(sulfur-*random*-(divinylbenzenes)); Δn, refractive index contrast; 1-PC, one dimensional photonic crystal; SiN, silicon nitride; SiO_2, silica; RIE, reactive ion etching; dB, decibel; FSR, free spectral range; FWHM, full width half max; TM, transverse magnetic; TE, transverse electric; ZnS, zinc sulfide; ZnSe, zinc selenide; ER, extinction ratio; NIL, nanoimprint lithography; BaF_2, barium fluoride; FIT, finite integration technique; FTIR, fourier transform infrared spectroscopy; NMR, nuclear magnetic resonance; $Hg_xCd_{1-x}Te$, mercury cadmium telluride; CO_2, carbon dioxide; NaCl, sodium chloride.

* Corresponding author at: Department of Chemistry and Biochemistry, University of Arizona, Tucson, AZ 85721, USA.
E-mail address: jpyun@email.arizona.edu (J. Pyun).

https://doi.org/10.1016/j.progpolymsci.2024.101865
0079-6700/

for the visible-NIR-SWIR spectrum (e.g., poly(methyl methacrylate) (PMMA-plexiglass), polycarbonate(PC), SU8, CYTOP), due to facile tunability of both optical and thermomechanical properties of these materials via molecular design, while retaining low absorption loss at telecom wavelengths in the SWIR at 1310 and 1550 nm [3,4]. Furthermore, photosensitive thin film polymeric materials are amenable to direct photolitographic processes for device fabrication in contrast to inorganic materials, such as, silicon nitride (SiN) or silicon (Si) [3–10]. However, optical polymeric materials generally possess much lower refractive index ($n \sim 1.3–1.6$) versus inorganic optical materials, along with poor IR transparency, particulalry in the MWIR and LWIR spectrum, which has limited deployment of these materials for IR optical applications [2].

A significant advance for IR optical materials was the discovery of *Chalcogenide Hybrid Inorganic/Organic Polymers (CHIPs)* by Pyun and Norwood et al. [2,11–17]. (also referred to as inverse vulcanized polymers, or organically modified chalcogenides in subsequent reports). These high sulfur content organopolysulfides are prepared by the direct copolymerization of elemental sulfur (S_8) (and selenium) with organic comonomers via a process termed *inverse vulcanization* [18–24]. The unusually high content of S-S bonds in the polymeric backbone imparts high RI values ($n \sim 1.7$ to 2.1), but also unprecendented optical transparency for synthetic polymers in the infrared spectrum due to the reduced organic content in the material and the shifted absorbances of S-S bonds outside of the MWIR and LWIR spectral windows. Furthermore, the reduced organic content in these high sulfur content polymers further mitigates the poor transparency in SWIR from 1300 to 1600 nm for most organic polymers arising from C-H, O-H and other bond vibrational overtones. These materials represent a novel hybrid class of optical materials possessing RI and IR transparency intermediate between classical inorganic optical materials, such as Ge, sapphire, or ChGs and organic optical polymers [15]. These materials retain the low cost benefit of polymeric materials (due to the very low cost of elemental sulfur from petroleum refining) and facile methods via solution or melt polymer processing for optical element fabrication, in contrast to semiconductors, glass, or ChGs. Bulk optics can be fabricated using classical melt casting and molding methods, along with lithographic or nanoimprint methods for thin film devices. Despite the recent work in this field, a critical challenge that remains is fabrication of optical elements and device components with these novel high sulfur content organopolysulfides. To date, the vast majority of research in inverse vulcanized *CHIPs* for photonics has focused on the synthetic chemistry of preparing new sulfur copolymers by designing new organic/hybrid comonomers for inverse vulcanization with S_8 to improve the IR transparency of these materials. Due to the yellow to red to black coloration of inverse vulcanized polysulfides, application of these materials for visible wavelength optical applications are limited, which has shifted the application focus for these materials to IR imaging and integrated photonics [2].

In this *invited PERSPECTIVE TREND*, we review the recent efforts on the successful fabrication of integrated photonics and optics for SWIR-MWIR-LWIR systems with inverse vulcanized *CHIPs* materials. Previous reviews on the inverse vulcanization of sulfur and IR optical polymers materials made from the inverse vulcanization of sulfur can be found elsewhere [2,18–24]. Recent fabrication methods for the high sulfur content thin films have been reported, such as Im et al., via sulfur chemical vapor deposition (sCVD) methods with S_8 and vinyl ethers/vinyl siloxanes, but the fabrication of bulk optics or integrated photonic components are still in progress [25–27]. Furthermore, recent work on two-photon photopolymerization with aliphatic thiol and norbornenyl monomers has been reported for the production of IR micro-optics and discussed elsewhere [28]. Due to the intended use of these optical polymers for IR optical systems, translation of these raw materials into precision plastic optics and integrated photonic device constructs is essential to evaluate the viabilty of these new optical materials *in operando* as functioning optical elements. Herein, we will review recent work within the past few years on the fabrication and characterization of IR optical components and photonic device constructs with inverse vulcanized *CHIPs* (Fig. 1). We will begin with solution processing methods to fabricate photonic crystal-Bragg reflectors for operation in the SWIR, followed by the photolithographic fabrication of single-mode waveguiding integrated photonic devices from inverse vulcanized *CHIPs* optical materials functioning at telecom wavelengths of 1310 nm and 1550 nm. The fabrication of MWIR polarizers and MWIR diffraction gratings using a combination of processing methods (e.g., photolithography to create masters, soft mold fabrication and casting) will then be discussed. Finally, fabrication of LWIR Frensel lenses and other micro-optics/diffractive optics will be discussed. To our knowledge, this is the first comprehensive review surveying the fabrication and characterization of functioning IR optical elements/devices across the SWIR-MWIR-LWIR spectrum made from inverse vulcanized *CHIPs*.

2. Materials for optical fabrication

While a broad family of organopolysulfides have now been prepared using inverse vulcanization, only a small subset of these materials have been successfully processed into viable optical elements and devices. Despite the extensive effort in the past decade to develop new inverse vulcanized organopolysulfides, difficulties remain in preparing materials possessing high thermomechanical performance and favorable polymer processing characteristics. Furthermore, the poor solubility of high sulfur content organopolysulfides from S_8 complicates precise structural characterization of many of these hybrid polymers [18–24]. Recent efforts on using both computational chemistry and structural characterization studies [29,30] point to these non-trivial challenges. Summarized below are the most widely studied organic monomers used to make sulfur-based polymeric optical components by inverse vulcanization, highlighting those materials demonstrated for optical fabrication. A more complete list of monomers and polymers used for inverse vulcanization for a wide range of applications can be found elsewhere [18–24]. The most widely studied and first monomer reported by Pyun et al. for inverse vulcanization is 1,3-diisopropenylbenzene (DIB) which after inverse vulcanization with S_8 affords poly(sulfur-*random*-(1,3-diisopropenylbenzene) (poly(S-*r*-DIB)). This amorphous glassy copolymer possesses glass transitions (T_g's) ranging from T = 35–50 °C with varying sulfur content and has been viable for both melt or solution processing, where copolymers with higher organic content can be rendered soluble in arene solvents [2,14,15,17,31,32]. Although poly(S-*r*-DIB) possesses fairly low T_g, the liquid form of this monomer, along with its low cost commercially has resulted in the most experimental work being done with this material for photonic device-optical element fabrication. The dynamic bonds in this material impart unusual rheological properties to this copolymer and it is one of the few examples of a Maxwellian polymer and rheologically "living" polymer [14,32]. DVB is commonly referred to as the regioisomeric mixture of 1,3- and 1,4-divinylbenzene (commercially sold) which affords poly(S-*r*-DVB) polymers with T_g's ranging from T = 50–110 °C based on sulfur composition and processing conditions [33–35]. NBD2 is made by the dimerization of norbornadiene with a nickel (0) cyclooctadiene (COD) catalyst ($Ni(COD)_2$) which affords one of the highest T_g's and thermal stability for sulfur polymers made by inverse vulcanization [15,32]. Poly(S-*r*-NBD2) behaves as a thermoset polymer, but is rheologically a dissociative covalent adaptable networks[32] Related sulfur copolymers arise from the inverse vulcanization of NBD or cyclopentadiene which afford lower T_g materials (T ∼ −12 to 45 °C) [36,37].

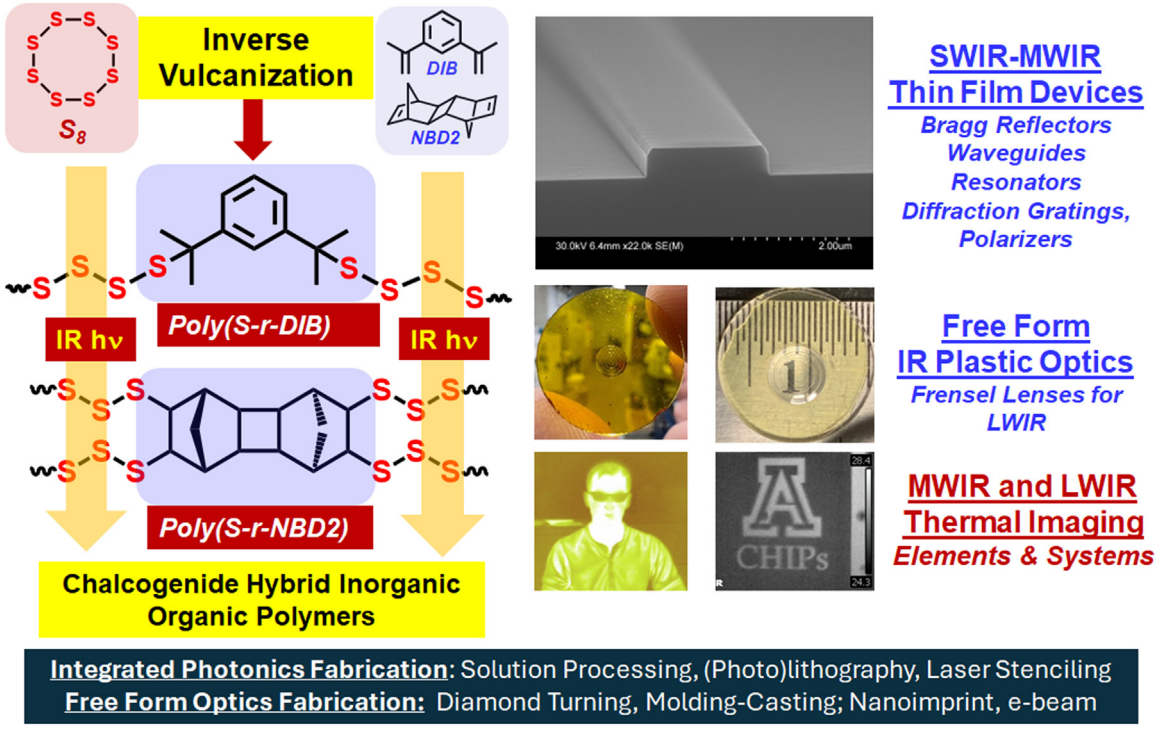

Fig. 1. Chalcogenide Hybrid Inorganic/Organic Polymers (CHIPs) made from inverse vulcanization of elemental sulfur with organic monomers (DIB, NBD2 shown here) for preparation of high sulfur content organopolysulfide optical polymers for fabrication of thin film based IR photonic device components and free-form plastic optics for IR thermal imaging. Adapted with permission from [13], Copyright 2014, Reproduced with permission from Wiley & Sons Publishing; [31], Copyright 2022, Reproduced with permission from Wiley & Sons Publishing; [77,13], Copyright 2024, Reproduced with permission from Wiley & Sons Publishing.

The high content of S-S bonds present in inverse vulcanized polysulfides impart ultra-high RI due to the high polarizability and molar refraction of S-units, where *n* can vary from 1.70 to 2.1 according to sulfur content [11,38]. Inverse vulcanized *CHIPs* exhibit improved optical transmittance (%T) in the SWIR due to the reduction of C-H-/C-C overtones which absorb strongly at the telecom wavelengths 1310 and 1550 nm. This holds significant potential for low cost, low loss integrated photonics due to reduction of optical propagation losses enabling improved and more efficient signal transmission in light guided device components; the high refractive indices also enable compact device structures increasing the density of photonic functions that can be incorporated [31]. Polymer waveguides, ring resonators and optical interconnects are among the primary optical components of interest here for both state-of-the-art telecom and future integrated photonics at longer IR wavelengths (MWIR) [39]. In the SWIR, particularly telecom wavelengths, numerous materials options are currently in use, which include SU8 polymers, plexiglass-PMMA and glass which dominate current markets [4]. New polymers for these products would require either marked enhancement of optical performance, or dramatic reduction of total device costs, which is feasible with S_8 derived polymers due to the low cost of sulfur [24]. Polymeric materials amenable to photopatterning using classical photolithography or nanoimprint methods particularly with high RI or reduced losses are advantageous for fabrication of polymer-based device components for integrated photonic device systems. Inverse vulcanized *CHIPs* for the MWIR have potential for both refractive optics and integrated photonics due to the reduced absorption intensity of the C–H bond vibrations at 3.3 μm. Other means to remove C–H bonds, such as fluorination, are feasible [4], but often are accompanied by disruptive immiscibility (processing incompatibility) with current chemical or polymer processing methods, as well as lower refractive indices. Recent interest in MWIR photonics for IR spectroscopic detection of gas sensing and other portable chemical sensing has prompted interest in lower cost devices based on polymers [40,41]. MWIR refractive optics based on lightweight and inexpensive optical polymers are of interest as alternatives to inorganic metal oxides, such as sapphire. The use of MWIR plastic optics for IR thermal imaging in this spectral window is feasible but is complicated by the need for enhanced thermomechanical durability at low/cyrogenic temperatures due to the use of MWIR photodetectors which require refrigeration. Similar benefits for improved LWIR transparency are imparted by a high content of S-S bonds in *CHIPs* which has generated interest in LWIR plastics optics for LWIR imaging. However, the intense LWIR absorption of organic moieties due to both fundamental and secondary bond vibrations (e.g. C-H, C-C, C=C, C-X) significantly reduces LWIR transmittance complicating direct fabrication of bulk LWIR plastic optics. Classic approaches to address the low LWIR transmissivity of plastic optics are being pursued through the design of flat diffractive optics approaches, as will be discussed.

3. SWIR photonics from 1000-3000 nm

3.1. Photonic crystals and bragg reflectors from CHIPs

The solubility of poly(S-*r*-DIB) at high organic compositions (> 50-wt% DIB) allows for dissolution in arene solvents enabling solution processing of these materials and multi-layer optical film fabrication. One dimensional photonic crystals (1-D PCs) (i.e., Bragg reflectors or dielectric mirrors) consist of alternating multi-layered films that afford high reflectivity by imparting large refractive index contrast (Δn) between layers and increasing the number of bilayers. A number of approaches using either homopolymer alternating bilayer constructs, or microphase separated block copolymer films have been developed to create these types of 1-D photonic crystals [15,42–47]. However, since most polymeric materials exhibit low refractive indices, highly reflective films require pre-

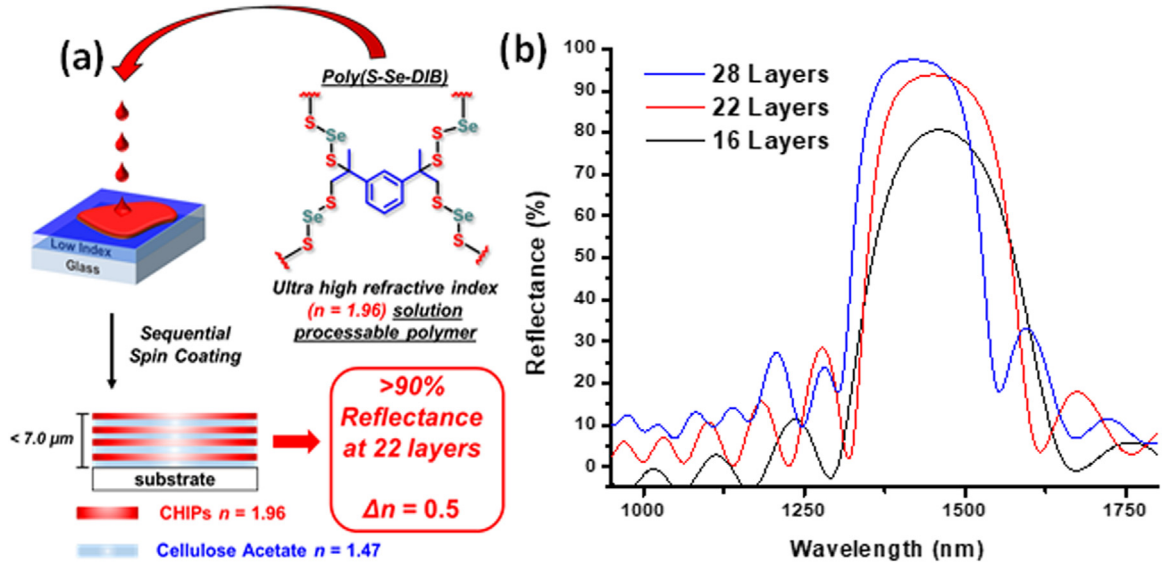

Fig. 2. (a) Fabrication of highly reflective all polymer 1-D photonic crystals from sulfur and selenium containing CHIPs copolymers that possess tunable NIR and SWIR (1.0–2.0 μm) reflectivity; (b) Bragg reflector spectra for devices with 16, 22 and 28 layers each with reflectance values at 1450 nm. Adapted with permission from [15], Copyright 2018 American Chemical Society.

cision polymer engineering methods since hundreds of layers are required. One such approach is melt-extrusion processing of disparate polymers to fabricate multi-layered films to achieve high reflectivity in the visible spectrum. Alternatively, the use of inverse vulcanized CHIPs possessing high refractive index (n > 1.75–2.1) enables pairing with conventional lower RI polymers that can be solution processed via spin coating to prepare highly reflective 1-D photonics crystals in the NIR AND SWIR [15]. In this case inverse vulcanization of S_8, elemental selenium (grey Se) and DIB afforded an ultra-high RI poly(S-*r*-Se-*r*-DIB) terpolymer (n = 1.96) which was solution processed with cellulose acetate (CA, n = 1.45) to fabricate 1-D PC (> 90 % reflectivity) by spin coating 20–30 bilayer films with poly(cellulose acetate) (CA, n = 1.45), which achieved a large Δn = 0.5 between the high index layer and low index layer for the first time with a wholly polymeric system (Fig. 2) [15]. Film thicknesses of individual layers of the poly(S-*r*-Se-*r*-DIB) and CA were around 200 and 300 nm, respectively, to achieve reflectivity in the SWIR (across 1–2.0 μm). Control of the peak reflection (λ) in a 1-D photonic crystal can be readily tuned by varying the thicknesses of the two layers in the Bragg reflector construct as described in Eq. (1)

$$t_H = \frac{\lambda}{4n_H} \qquad t_L = \frac{\lambda}{4n_L} \tag{1}$$

where t represents thickness (nm), n is refractive index and H and L denote "high" and "low" index components, respectively. The advantages of using a high RI polymer are evident in the reduced number of layers required to achieve high reflectivity, which would require high precision engineering processing methods to create much thicker multi-layered films when working with smaller refractive index contrast. Elegant work by Comoretto et al., has utilized higher RI inverse vulcanized polysulfides prepared using vinylic thiophene comonomers to provide 1D-PCs with high levels of reflectivity [47].

3.2. *Integrated photonic waveguiding devices from* CHIPs

Optical waveguides, in this case polymer waveguides, are fundamental optical elements ubiquitous in any photonic integrated circuit (PIC) that all require the use of low-loss, single mode optical waveguides. Synthetic polymers have long been used materials for polymer waveguiding components for integrated photonics [3,4]. Despite the numerous fabrication advantages associated with optical polymers, these materials possess relatively low refractive index (RI) (n ~ 1.3 – 1.6 at telecom wavelengths), versus the state of the art inorganic material counterparts (e.g., silicon nitride (SiN), lithium niobate (n ~ 2.0–2.2), Hence, on-chip integrated photonic components (e.g., waveguides or ring-resonators) made with these polymeric components require much larger feature sizes beyond what is tenable for numerous on-chip devices requirements. Hence, there is a clear need for high RI polymers (n >> 1.6 at telecom at 1310 nm and 1550 nm) that are amenable to thin film processing and high throughput nano/microfabrication techniques (e.g., photolithography) for integrated photonics.

To address this need, Pyun & Norwood et al. fabricated singe-mode polymer waveguides using poly(S-*r*-DIB) (with 70 wt% sulfur) as the higher RI core layer in these photonic device components due to the higher RI (n = 1.75 at 1550 nm) and lower optical losses of these materials relative to state-of-the-art polymer waveguide materials [31]. The polymer waveguide optical performance requires measurement of the propagation loss which has contributions from both the optical absorption loss and scattering intrinsic to the material and extrinsic scattering loss arising from side-walls and other interfacial roughness attributed to the defects associated with the fabrication process [3,4,48–51]. The goal of the waveguide fabrication process is to have the propagation loss limited by material absorption alone, with negligible contribution from the scattering loss. Hence, minimzation of sidewall roughness during waveguide fabrication is essential to polymer waveguide fabrication with low propagation loss. Single mode waveguides using poly(S-*r*-DIB) as the core material were fabricated with cross-sectional dimensions of 2 μm width and 0.45 μm height to ensure single-mode guiding. To achieve large refractive index contrast (Δn ~ 0.4), cladding layers of SiO_2 (n = 1.44 at 1550 nm) and ZPU (n = 1.43 at 1550 nm) were used with the poly(S-*r*-DIB) core layer, where a ZPU film was solution cast as the top cladding layer (thickness ~ 4 μm) followed by UV curing under N_2 atmosphere. Lithographic structuring of the core layer was achieved by spin coating of poly(S-*r*-DIB) onto SiO_2 bottom clad films on a carrier Si substrate, followed by electron beam (e-beam) lithography of the photoresist layer (maN2403), and reactive ion etching to create the desired device architecture. SEM of poly(S-*r*-DIB) waveguides

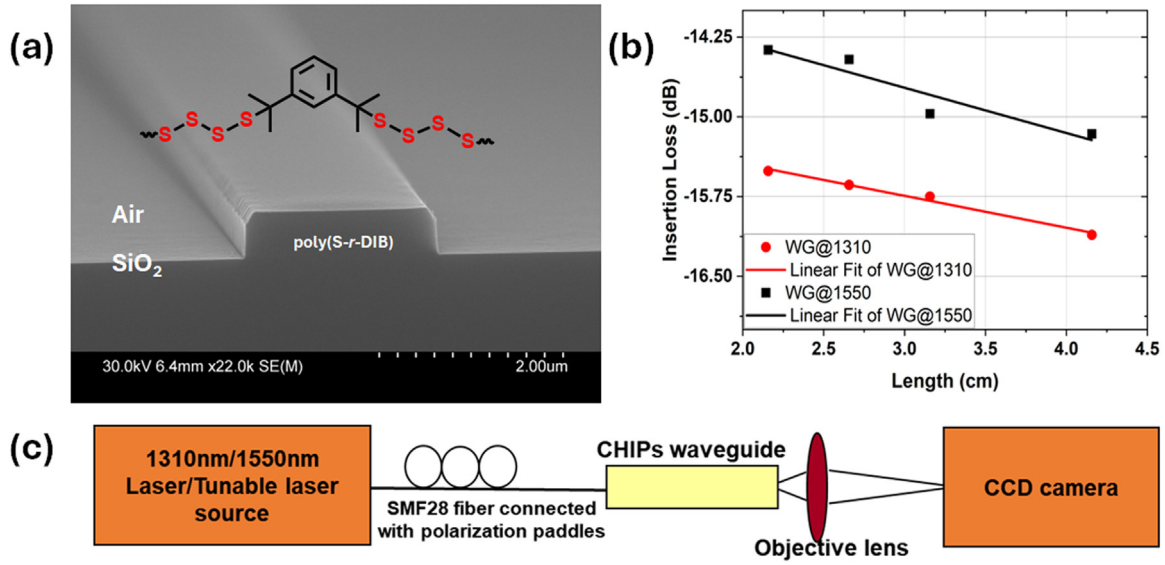

Fig. 3. (a) SEM image of e-beam lithographically patterned poly(S-*r*-DIB) core layer with chemical structure of the sulfur copolymer overlaid on top. Due to excellent fabrication methods, very smooth core layer side walls were prepared from this process; (b) characterization of propagation loss in this poly(S-*r*-DIB) and ZPU waveguide by the cutback method at 1310 nm and 1550 nm wavelength; (c) experimental setup for imaging the *CHIPs* waveguide mode profile. For measuring the power, the output side was replaced with SMF28 fiber and a power meter. Adapted with permission from [31], Copyright 2022 Wiley & Sons Publishing.

on SiO_2 confirmed that the desired feature sizes were obtained, along with very smooth sidewall features indicating very favorable nanostructuring with reactive ion etching (RIE) (height = 450 nm, width = 2 μm, Fig. 3a, ZPU top cladding layer absent). A series of serpentine waveguides with lengths varying from 20 mm to 40 mm were made on the same sample to measure the propagation loss via classic cutback methods. The power was measured for waveguides of varying length, where as a reference, input and output fibers were coupled together with index matching oil to determine the reference power (Fig. 3c). The total insertion loss was calculated by subtracting the reference power from the output power for each waveguide. The final insertion loss when plotted against the length of each device gave a linear curve with excellent goodness of fit, R^2 value > 0.95 and estimated propagation loss of 0.3 dB/cm at 1310 nm and 0.42 dB/cm at 1550 nm wavelength, as shown in Fig. 3b. These optical losses were considerably less than conventional hydrocarbon polymer based waveguides that generally exhibit a lower loss limit of ~ 1 dB/cm at 1550 nm due to the presence of strong vibrational overtones from C-H bonds at telecom wavelengths. The observed reduction of the propagation loss in poly(S-*r*-DIB) below 1 dB/cm can be directly attributed to the high fraction of S-S bonds in these organic/inorganic hybrid polymers and the reduced fraction of organic comomer units [31].

3.3. *Ring resonator integrated photonic devices from* CHIPs

Ring resonators are critical photonic device components that are able to optically filter certain wavelenghts of light through control of ring dimensions, which have use for optical modulators, dense wavelength division multiplexing, optical delay lines, biosensing, and high quality optical cavities in general. Ring resonator performance is highly sensitive to the quality of the micro/nanofabrication methods, where ring resonator feature sizes are critically associated with the RI of the active core material as higher RI in the core enables reduction of the ring radius with engendering radiative bend losses [50]. Polymer-based ring resonators require ring resonator radii exceeding 1 mm when fabricated with classical optical polymers possessing lower RI ($n < 1.6$) [46]; these large radii limit device density on the photonic chip. Hence, use of high RI *CHIPs* from poly(S-*r*-DIB) ($n = 1.75$) by Pyun & Norwood to enabled dramatic reduction of the ring-resonator radii to below 1.0 mm, as demonstrated in all pass ring resonators, the most widest used type in integrated photonics [31]. For this ring-resonator device architecture, input light from an external laser is launched into the input bus waveguide which guides the light across the length of the chip where a ring resonator of fixed radius is fabricated proximal to the bus waveguide (typical gap between bus and ring > 1 μm). Design of the ring cavity features (shape, dimension) and gap dimensions between the input bus waveguide enable precise tuning of the resonance wavelength and the free spectral range (FSR) of the final device where narrow linewidth of the resonance peak (i.e. the full width half maximum (FWHM)) is targeted. The ratio of the resonance wavelength to the FWHM gives us the ***Q factor of the ring***, which is a critical parameter to assess the quality of the fabrication as well as the effectiveness of the coupling schemes employed in the device design. Furthermore, the ***finesse*** of the ring resonator (the ratio of FSR to the FWHM) is an important parameter in conjunction with the Q-factor in evaluating ring-resonator device performance. While polymer based high Q resonators have been reported, these devices typically also exhibit low finesse, which limits the their utility. Due to both the solution processability and high RI of poly(S-*r*-DIB), high Q and high finesse polymeric ring-resonators could be fabricated with a dramatically reduced ring radius of 200 μm to obtain a free spectral range (FSR) of 1.1 nm with a resonance wavelength, λ_0 of 1550 nm (see SEM image, Fig, 4a). Based on the resolution of e-beam resist, aspect ratio, and ease-of-fabrication, the gap between the straight section and the ring in the coupler region was optimized between 0.3 μm to 1.1 μm to allow for the determination of the critical coupling of the ring with the straight coupler section since optimization of device performance requires efficient coupling to achieve the largest extinction ratio. The fabrication of the poly(S-*r*-DIB) ring-resonator was achieved using similar solution processing and e-beam lithographic methods as described for poly(S-*r*-DIB) polymer waveguides reported in Fig. 3.

Critically coupled operation was observed for a 1 μm gap, evidenced by the sharp decrease in resonance linewidth, where the linewidths of the resonance peaks decreased from 1 nm to 0.02 nm for the critically coupled case along with very high extinction ratios (Fig. 4b). The resonance (λ_0) was centered around

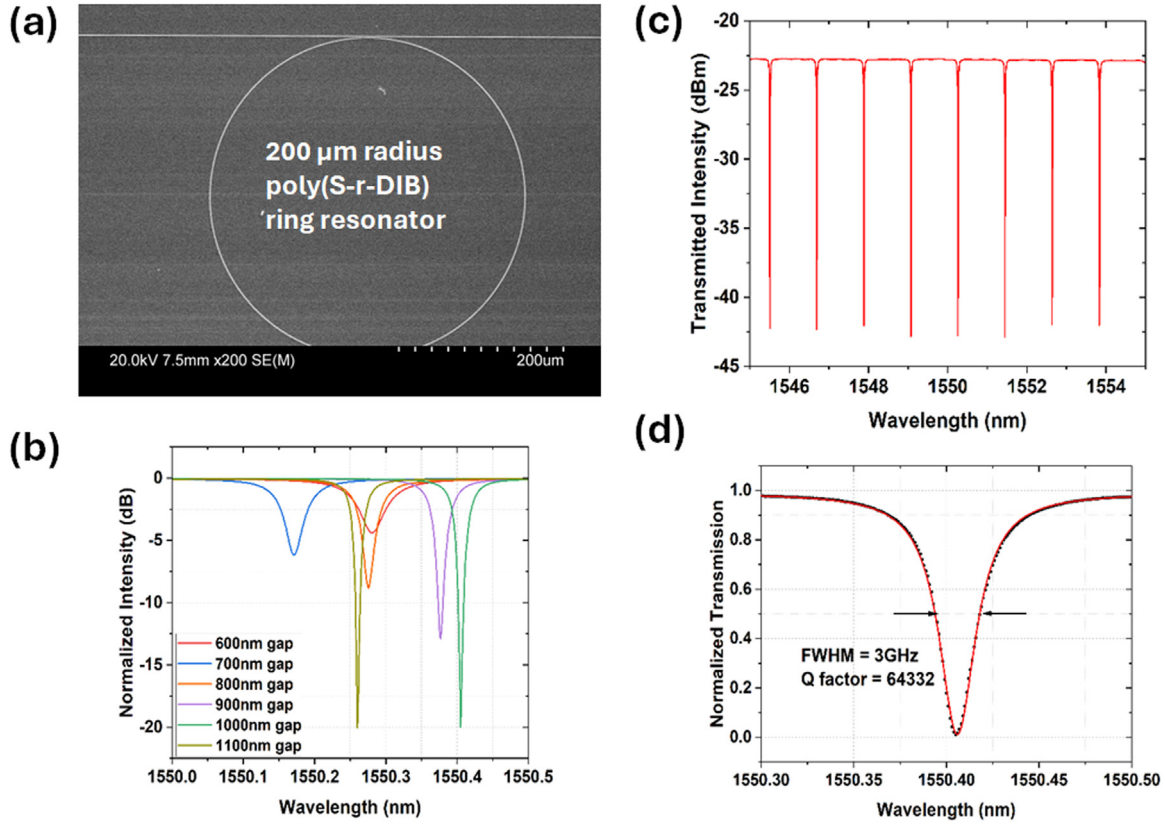

Fig. 4. (a) SEM of poly(S-r-DIB) ring resonator with radius = 200 µm; (b) normalized intensity of ring resonators with varying gap; the slight shift in resonance peak was due to fabrication imperfections and minimal change in effective index; (c) output spectrum for critically coupled ring with 20 dB extinction ratio and narrow linewidth; (d) normalized transmission for central peak at 1550.4059 nm with full width half maximum of 3 GHz corresponding to a Q factor of 64,332. Adapted with permission from [31], Copyright 2022 Wiley & Sons Publishing.

1550.4059 nm with an FSR of 1.1 nm which is very close to the designed value of 1550 nm and 1.09 nm respectively. The normalized resonance dips are fit to a Lorentzian function, giving us a ***Q ~ 65,000*** with over 20 dB extinction ratio and a ***high finesse value of 45*** for the cavity, as shown in Fig. 4c. To our knowledge this is the first result demonstrating high performance ring-resonators fabricated from a high RI optical polymers that enabled reduction of ring-resonator radii while still retaining high Q-factors [52]. While the fabrication of high Q-ring resonators from polymers have been reported, these examples require significantly larger ring radii (1–5 mm vs the 200 µm for poly(S-*r*-DIB) ring) and very low finesse (~2–8) [31]. The photonic devices demonstrated in this work highlight the potential of using processable *CHIPs* for photonic integration, especially in low-cost wavelength division multiplexed systems targeted at high bit rate artificial intelligence data center applications. These advantages in conjunction with the low cost of these optical polymers due to the use of elemental sulfur point to the potential for scaling up the fabrication to wafer level processes in realizing all-polymer photonic devices.

4. MWIR photonics from 3-5 µm

The development of MWIR integrated photonics and refractive optics is technologically important for numerous current and emerging applications. MWIR thermal imaging as alluded to previously is of tremendous importance for defense applications in high quality night-time vision and sensing [2]. However, fabrication and demonstration of a MWIR plastic lenses, or other MWIR plastic optics *in operando* has not been extensively developed, likely due to the low temperature/cyrogenic conditions required for MWIR photodetectors. Conversely, MWIR integrated photonics is an emergent technology that has generated significant interest for chemical sensing and portable IR spectroscopic detection of organic compounds, where the spectral window around 3.3 µm-4.2 µm/3000–2200 cm^{-1} is of particular interest due to C-H bond and C=O vibration stretching in this MWIR range. However, the development of MWIR transparent media that are also amenable to manufacturing fabrication methods remains a critical challenge for this application. Hence, the development of MWIR polymeric waveguiding components and diffractive optical elements (polarizers, gratings) has been of interest to enable further advancement of MWIR integrated photonics.

4.1. MWIR polarizers

MWIR polarimetry is of importance for numerous MWIR thermal imaging system to enhance contrast and imaging resolution, as polarized light is sensitive to topographical and textural features in complex imaging environments. Hence, MWIR polarizers with high sensitivity are desirable which requires this device component exhibit both a high transmission of the linearly polarized MWIR light in the transverse magnetic (TM) and transverse electric (TE) modes and a high extinction ratio (ER), where the ER is determined by the ratio of TM to TE. Hence, MWIR polarizers with higher ER values are desirable to allow for complete TM transmission and TE occlusion to afford maximal polarization imaging performance [53,54]. State-of-the-art MWIR polarizers are fabricated from inorganic IR transmissive materials (e.g., Ge, Si, zinc chalcogenides (ZnS, ZnSe), amorphous chalcogenide glass) which possess outstanding optical properties (high RI, high IR%T), but are intrinsically expensive and require high energy input processes (e.g., interference lithography

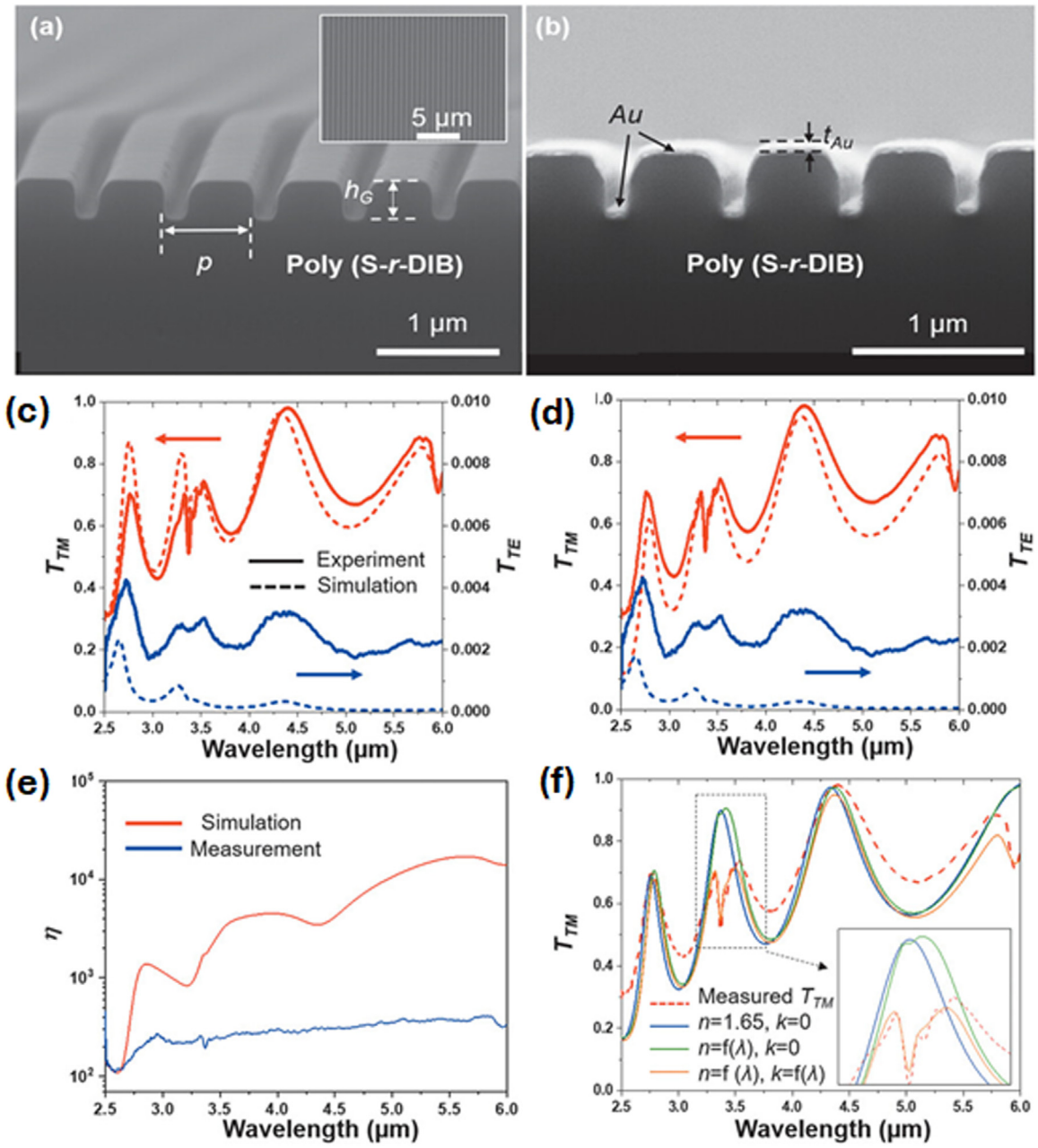

Fig. 5. SEM images of thermal-nanoimprinted poly(S-r-DIB) MWIR grating (a) before and b) after the Au deposition to prepare the polarizer (c,d)The trends of the measured transmissions (solid lines) compared to the FIT-simulation (dashed lines) for poly(S-r-DIB) polarizer (The comparison of the measured transmissions (solid lines) to the FIT-simulation (dashed lines). (e) Comparison between the measured experimental η of the poly(S-r-DIB) polarizer and simulated η. (f) Simulated TTM of sample structure with modified geometry using a constant refractive index, $n = 1.65$, the measured complex wavelength-dependent refractive index by using spectroscopic ellipsometry, $n(\lambda) + i \cdot k(\lambda)$, as depicted, and the wavelength-dependent refractive index without the loss in poly(S-r-DIB), $n(\lambda)$. Adapted with permission from [56], Copyright 2018 Wiley & Sons Publishing.

and etching) to fabricate into optical elements [55,56]. Hence the fabrication of a polymeric MWIR polarizer was highly desirable.

The first report on MWIR polarizer fabrication was demonstrated by Ryu et al., by spin coating thin films of poly(S-*r*-DIB), thermal nanoimprint lithography of a bilayer polymer polarizer and Au deposition to prepare periodic grating geometries [56]. Subsequent optimization of spacer thickness and grating geometries (e.g., pitch, width, and heigh) enabled improved transmission and higher extinction ratio polymer polarizers [57]. MWIR poly(S-*r*-DIB) polarizers of optimal dimensions (height = 0.43 μm, width = 0.55 μm, pitch = 0.7 μm, 0.055 μm Au overcoat; see Fig. 5a, b for SEM imaging) were determined using the CST Microwave Studio (CST-MWS), which is based on a finite integration technique (FIT). The TM- and TE-transmission spectra were measured by Fourier transform infrared spectroscopy (FTIR) and compared with the simulation results, where reduced experimental transmission intensities were observed. These lower TM values were most closely correlated to slightly curved features at the base of molded polymer polarizer features as seen in the SEM cross-section of nanoimprinted poly(S-*r*-DIB) polarizers (Fig.5a,b), along with the ZnSe wire-grid polarizer used to filter the TE-polarized incident wave in these measurements. Hence, the experimental extinction ratios (η) at 3, 4, and 5 μm for these poly(S-*r*-DIB) MWIR polarizers (($\eta_{\text{experimental}}$ = 245, 305, 351) were also lower than the

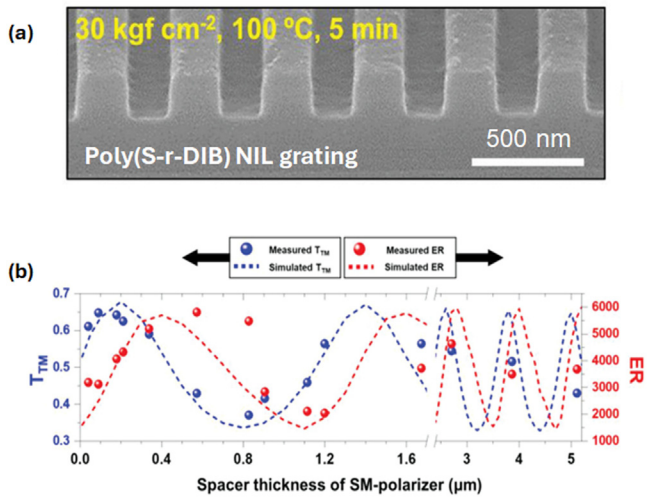

Fig. 6. (a) SEM images of poly(S40-r-DIB60) 1D nano-gratings fabricated under the final thermal NIL conditions—a pressure of 30 kgf cm−2, a temperature of 100 °C, and an imprinting time of 5 min. (b) Simulated and measured TTM and ER of the SM-polarizer as functions of the spacer thickness at 4 μm wavelength. The dashed lines and symbols indicate the simulation and measurement results, respectively. Adapted with permission from [58], Copyright 2018 Wiley & Sons Publishing.

simulated extinction ratio values ($\eta_{\text{simulatedl}}$ = 1149, 4494, 10,629) at these MWIR wavelengths [56].

Enhanced MWIR polarizers from thermal nanoimprint lithography of poly(S-r-DIB) were demonstrated by Wie et al., via high precision fabrication methods which improved the edge-sharpness of imprinted grating features when further overcoated with Au (Fig. 6a) [58]. The grating spacer thickness was controlled via low cost spin-coating processes, followed by thermal NIL of poly(S-*r*-DIB) with a specialized Ormomer-PET master. This process afforded NIL features with sharp right-angled edges by control of the wetting dynamics of the polymer in the mold, i.e., overcoming the energy barrier of the Cassie–Baxter state, originating from the high surface tension and viscosity of the sulfur polymer. Higher NIL temperatures and optimization of thermal pressure and time afforded high fidelity 1D gratings, giving improved MWIR polarizers after Au deposition onto these sharp-edged patterned gratings. These MWIR polarizers gave high TM transmission as determined from IR spectroscopy (TM = 0.65, 0.59, and 0.43) and remarkably high ER in close agreement with simulated ER values ($\eta_{\text{experimental}}$ = 3.12 × 10^3, 5.19 × 10^3, and 5.81 × 10^3 at 4 μm for spacer thicknesses of 90, 338, and 572 nm (Fig. 6b). These values are superior to those of commercial semiconductors, metal salt, or chalcogenides MWIR polarizers such as BaF_2, ZnSe, and KRS-5, (ER ~ 0.15 × 10^3; TM ~ 0.50–0.65) and around 20x larger ER values than the prior poly(S-*r*-DIB) MWIR polarizer.

4.2. Diffraction gratings

The development of MWIR diffraction gratings, particularly for operation in the MWIR 3.3–4.2 μm/3000–2200 cm^{-1} window is of significant interest for chemical sensing via IR spectroscopic methods with miniaturized, or portable devices [59–61]. Diffraction gratings are essential optical components in numerous spectrometers (e.g., for IR spectroscopy) taking broadband light sources and spatiallydispersing the wavelengths over the wavelength range of interest. Diffraction gratings are structurally similar to polarizers, as discussed in the previous section, as both of these optical elements require the fabrication of periodic structures with controllable feature size. Polymeric MWIR gratings have not been widely developed due to the requirement of removing all C-H bonds in these materials to avoid background absorption in this spectral window. Hence, the concept of both sulfuration and deuteration of optical polymers was demonstrated by Pyun et al., as replacement of C-H for C-D bonds shifts and reduced the intensity of vibration resonances from ~3.3 μm (~3000 cm^{-1}) to 4.2 μm (~2200 cm^{-1}) in conjunction with the benefits of a high fraction of S-S bonds [27]. While deuteration of polymers has long been known to enhance contrast in morphological studies with *proteo* polymer blends, the development of new uses for deuterated polymers remains limited [62,63]. Hence, a perdeuterated 1,3-diisopropenylbenzene (d_{14}-DIB) was synthesized with a very high level of purity and deuteration (99.2 %) beginning with deuterated d_8-toluene executing the seven-step total synthesis using only deuterated NMR solvents as reagents (Fig. 7a) [30]. This synthesis was particularly challenging due to the high enrichment levels of deuterium at every position, the limited number of possible *deutero* precursors available and the possibility of undesirable H/D exchange. However, d_{14}-DIB was synthesized in gram quantities and enabled direct structural, computational and mechanistic studies comparing the inverse vulcanization of S_8 *proteo* DIB vs *deutero* DIB for the first time, which revealed numerous kinetic isotope effects on the polymerization mechanism and microstructure of the resulting poly(S-*r*-DIB) vs poly(S-*r*-d_{14}DIB) copolymers [30]. The benefits of very high level of deuteration of organic monomers for MWIR photonics was evident in the comparative IR spectroscopy of *proteo* vs *deutero* DIB where the C-H vibration absorptions from 3.3 to 4.0 μm are completely shifted to 4.2–4.8 μm, along with a reduction in peak absorption intensity (Fig. 7b). IR spectroscopy of *proteo* vs *deutero* poly(S-*r*-DIB) (250 μm films) further confirmed similar C-H vs C-D spectral trends as for the DIB vs d_{14}-DIB monomers, where a nearly 60x enhancment in IR transmission (MWIR%T) at 3.3–3.4 μm was observed for the C-D *deutero* poly(S-*r*-d_{14}-*DIB)* vs the *proteo* poly(S-*r*-DIB) material (Fig. 7c). The presence of trace 0.8 % *proteo* impurities carried into the sulfur copolymer from the d_{14}-DIB monomer (99.2 %), resulted in the appearance of small C-H peaks at 3000 cm^{-1} [30]. Hence, this level of deuteration in the sulfur copolymer precluded the possibility to use these as discrete MWIR plastic lenses, or windows for MWIR imaging. However, this level of deuteration was more than sufficient for thin film MWIR photonics which was pursued for fabrication of novel MWIR polymeric diffraction gratings.

MWIR optical diffraction gratings were designed and fabricated to demonstrate the utility of sulfuration and deuteration in a moldable polymeric medium for MWIR spectroscopy, where a MWIR laser operating at 3.39 μm was required to enable comparison of both *proteo* and *deutero* poly(S-*r*-DIB) materials (Fig. 8). In this experiment, the successful generation of diffracted wavefront pattern at 3.39 μm would only be possible through the *deutero* poly(S-*r*-DIB) grating since the *proteo* poly(S-r-DIB) diffractive grating was completely opaque at these MWIR wavelengths. MWIR polymer gratings with 250 μm thick film of the poly(S-*r*-DIB) copolymer were fabricated, since in this thickness regime the *deutero* poly(S-r-DIB) exhibited high transmission (~60 % T) at 3.39 μm vs the non-transmissive (~ 0 % T) *proteo* film (**see** Fig. 7c) The sulfur copolymer diffraction gratings were designed with a 6 μm periodicity, 1 μm in height (h) and 200 μm thickness with a 50 μm flash layer (see Fig. 8c for SEM image) were chosen to maximize MWIR first-order diffraction spots, due to the low intensity of MWIR photons and MWIR cameras used in this experiment (Fig. 8a). This MWIR experiment required significant effort to acquire a MWIR laser sources operating near 3.3 μm and MWIR thermal camera to enable viewing of the MWIR diffracted wavefront pattern. To confirm broadband operation of both *proteo* and *deutero* poly(S-*r*-DIB) diffraction gratings, irradiated in the visible, NIR and MWIR with 633 nm, 976 nm, and 3.39 μm monochromatic laser sources was conducted. Both *proteo* and *deutero* sulfur polymer gratings

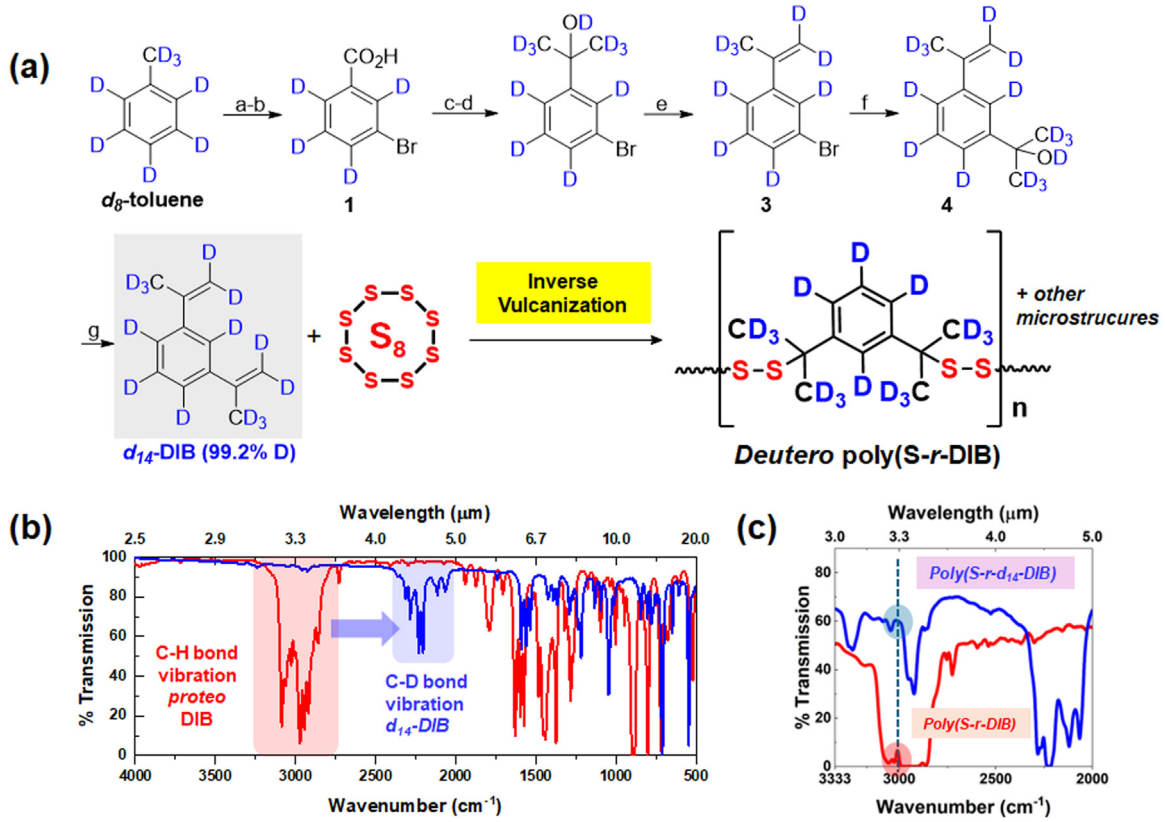

Fig. 7. (a) Total synthesis of d_{14}-DIB from d_8-toluene: a) $KMnO_4$, Na_2CO_3, H_2O, 120 °C (54 %), b) $KBrO_3$, K_2SO_4, H_2O (94 %), c) MeOH, H_2SO_4 (86 %), d) CD_3MgI, Et_2O then CH_3OD (63 %), e) p-TsOD, benzene, 110 °C (53 %), f) n-BuLi, Et_2O, D_6-acetone, −78 to 0 °C, then CH_3OD (64 %) and g) p-TsOD, benzene, 80 °C (54 %), followed by inverse vulcanization with S_8 (50-wt%,70-wt%), 165 °C. (b) Stacked FTIR (A) transmission spectra of DIB (red) and d_{14}-DIB (blue) from 2.5 to 20 μm; (c) stacked IR transmission spectra of proteo vs deutero poly(S-r-DIB) films (250 μm thick), dashed line at 3.3 μm indicated a 60-fold difference in IR transmission between proteo vs deutero poly(S-r-DIB). Adapted with permission from [30], Copyright 2023 American Chemical Society.

performed identically in the visible spectrum at 633 nm (affording both low- and high-order diffraction spots, Fig. 8b) and in the NIR at 976 nm, however, only the *deutero* poly(S-*r*-DIB) optical grating produced a diffraction pattern with zeroth- and first-order MWIR spots at 3.39 μm, (Fig. 8d), whereas the *proteo* optical grating showed neither transmission nor diffraction (see Fig. 8e) due to C-H bond vibrations in the polymeric medium. The experimentally measured diffraction angle ($\theta_{exp} = 33.7°$) of the MWIR *deutero* poly(S-*r*-DIB) grating at 3.39 μm was found to be in good agreement with the theoretical value ($\theta_{theoretical} = 34.5°$) based on the grating dimensions described in Fig. 8a [30].

5. LWIR imaging (7–14 μm)

IR thermal imaging can be conducted in the LWIR (7–14 μm) spectrum and is primarily based on detecting black body radiation emitted by imaging targets. LWIR photons can be detected using bolometric sensing, or low bandgap semiconductor detectors at these respective wavelengths. LWIR imaging systems can be significantly less expensive with the use of microbolometer sensors based on materials with large temperature dependent resistance (e.g., silicon, or vanadium oxide semiconductors) however, the trade off can be reduced sensitivity vs mercury cadium telluride ($Hg_xCd_{1-x}Te$) or other semiconductor LWIR photodetection, but such detectors require expensive cooling for LWIR detection [1,2]. At the same time, the limited number of available IR transmissive materials for optical elements (e.g., windows & lenses) remains a significant expense for these LWIR imaging systems based on expensive materials, such as germaniuam (Ge) or chalcogenide glasses (ChG's). While these more expensive LWIR imaging systems are widely used for defense or aerospace applications, deployment of this technology for non-defense consumer markets in transporation, housing and personal electronics remains stifled by the high cost associated with the IR cameras and electronics. This is particularly an issue for MWIR and LWIR imaging systems that use semiconductor photodetectors that require low temperature refrigeration to suppress background dark current due to the low bandgap of the detectors [2]. While low cost and moldable plastic optics have been desirable for use as LWIR transmissive materials, the strong MWIR and LWIR absorption of organic materials is an intrinsic limitation of this class of materials for IR optics. The one exception is polyethylene (PE), where the chemical simplicity of this material (e.g., only sp^3 C-C, C-H bonds) affords good LWIR transmission due to the sharp degenerate spectral peaks that converge around the conventional spectral window employed for LWIR imaging (8–12 μm); at the same time the scattering caused by the semicrystallinity of PE is greatly reduced in the LWIR compared to the visible. In contrast, while commodity amorphous optical polymers, such as, poly(methyl methacrylate) (PMMA-„plexiglass“) or polycarbonate (PC) are very transparent for visible,or NIR wavelength applications [64,65], they are opaque in the LWIR region [2]. To date fabrication of LWIR refractive optics cannot be done with thick optical elements due to low LWIR transparency of these materials, as previous discussed. Hence, researchers have pursued flat diffractive optics which include Fresnel lenses[66] and more complex metalens systems [67,68]. LWIR diffractive optics using PMMA [69], or hybrid polymer-silicon based materials[70] have been demonstrated, which can then be prepared as thin film optical lenses (thicknesses below 0.1 mm) to circumvent the intrisically low LWIR transparency of these organic optical materials.

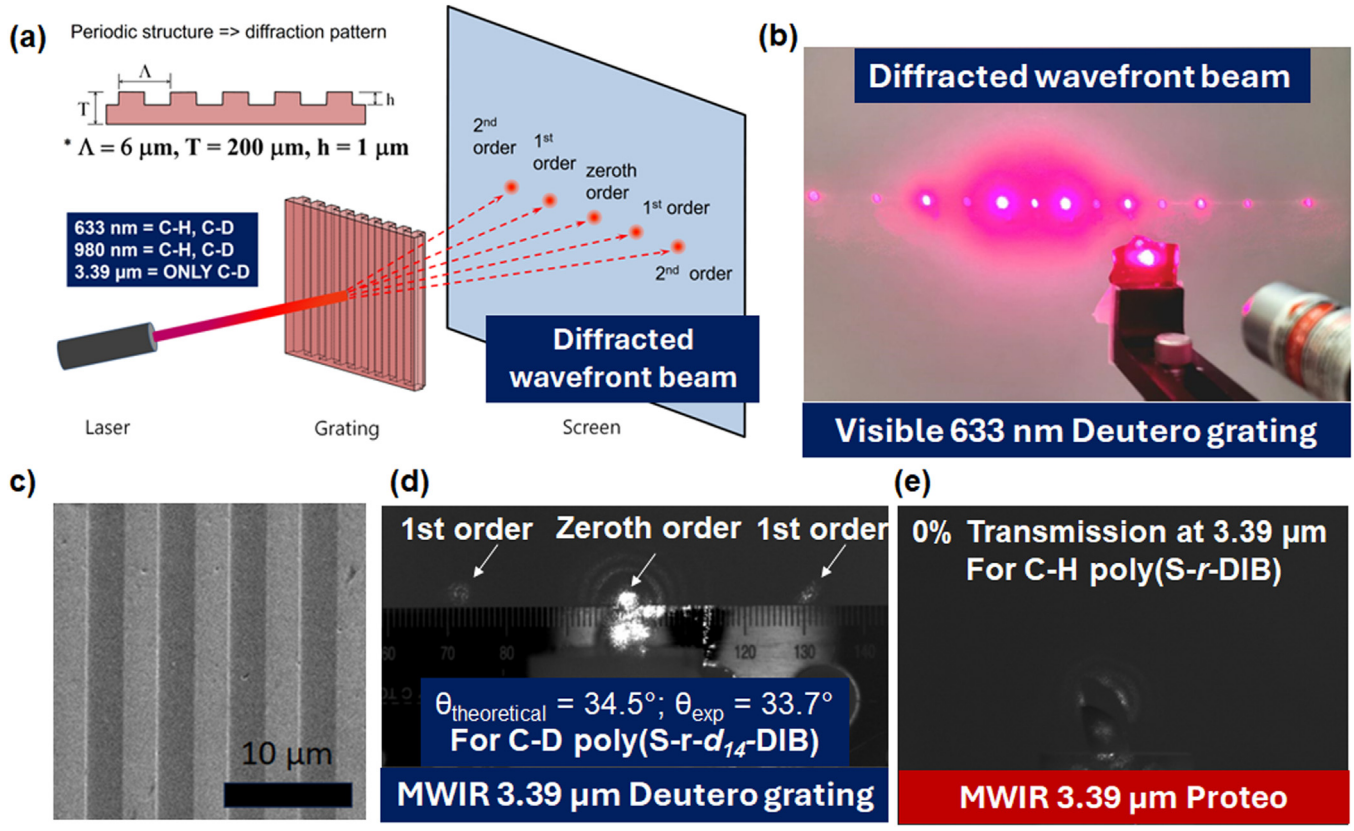

Fig. 8. (a) Design of optical grating, and schematic for diffraction grating experiment in the VIS-NIR-MWIR; (b) optical diffracted beam through the poly(S-*r*-d_{14}-DIB) optical grating (total thickness = 250 μm with 50 μm flash layer) in the visible spectrum with 633 nm irradiation; (c) SEM image of poly(S-r-d_{14}-DIB) diffraction grating; (d) MWIR thermal image of 3.39 μm generated diffracted beam of zeroth and first orders through the poly(S-*r*-d_{14}-DIB) optical grating (total thickness = 250 μm); (e) featureless MWIR image of 3.39 μm generated diffracted beam through the proteo poly(S-*r*-DIB) optical grating (total thickness = 250 μm, with 50 μm flash layer). Adapted with permission from[30], Copyright 2023 American Chemical Society.

Polyethylene (PE) based Fresnel lenses for LWIR imaging have been commercialized and are currently the only viable polymeric LWIR plastic optic [71]. However, PE has significant limitations as an IR transmissive material, which include limited processabilty for optical fabrication (arising from semi-crystallinity) which leads to reduced transmission from light scattering, and low refractive index.

Recent efforts by numerous groups have focused on the design of organic comonomers for the inverse vulcanization process to prepare inverse vulcanized *CHIPs* with enhanced LWIR transparency using high sulfur content polymers derived from S_8 and the inverse vulcanization process, which now include, tetravinyltin [72], dimeric norbornadiene (NBD2) [16], aryl halides [73], benzene-1,3,5-trithiol [74], 1,3,5-trivinylbenzene[75] episulfides [76], and cyclopentadiene [37]. However, an intrinsic limtiation with S_8 derived *CHIPs* is the requisite organic comonomer phase (typically 10–50 wt% in the material), which ultimately limits its LWIR transparency relative to Ge, or ChG's. Pyun and Norwood et al., developed poly(S-*r*-NBD2) in 2019[16] which was found to exhibit excellent thermomechanical properties (T_g's > 100 °C at both 50-wt% and 70-wt% sulfur) and significantly enhanced LWIR%T compared to poly(S-*r*-DIB) copolymers and standard commodity optical polymers (e.g., PMMA). Due to the favorable combination of thermomechanical, optical and melt processing characteristics, LWIR Fresnel lenses from poly(S-*r*-NBD2) were developed by this same group to demonstrate for the first time successful fabrication and *in operando* characterization of LWIR plastic optics, as detailed below [77].

A basic benctop LWIR imaging system was constructed using a hotplate/stirrer as the IR black body source in conjunction with a custom-designed PMMA target where focusing was achieved with molded sulfur copolymer lenses into a LWIR microbolometer detector (Fig. 9a). Pyun and Norwood pioneered the fabrication of free standing windows of inverse vulcanized polymers for qualitative MWIR and LWIR transparency assessments using MWIR photography of human subjects [13], or with the aid of PMMA laser stenciled imaging targets [16]. This practice was adopted in the above mentioned reports on sulfur polymer based films, or windows. However, the design, fabrication and characterization of LWIR plastic optics *in operando* was a critical milestone required to validate these new optical polymers for LWIR imaging. Furthermore, there remained a need for establishment of complete laboratory scale LWIR imaging systems fitted with new LWIR plastic lenses to enable rigorous structure-property-performance assessments of new inverse vulcanized polymers.

To enable facile, but uniform evaluation of LWIR imaging experiments, this team further developed on our concept of using PMMA imaging targets made by carbon dioxide laser stencil writing into plastic sheets. A simple target pattern fabricated by CO_2 laser writing into a PMMA sheet of hollow lines and numbers varying from 1 to 3 mm in length and width and the word, *Infrared*, which when placed in front of a blackbody radiator, would create a well-defined optical resolution test chart, which was referred to as the University of Arizona Infrared Target (UA-IR target, Fig. 9b–d). The standard USAF target cannot be used for LWIR experiments since the glass substrate is highly absorbing in the LWIR unless used in a reflective imaging modality. The LWIR detector chosen for this lab-scale system was the FLIR Lepton 2.5 microbolometer, which exhibited acceptable LWIR detector sensitivity from 8 to

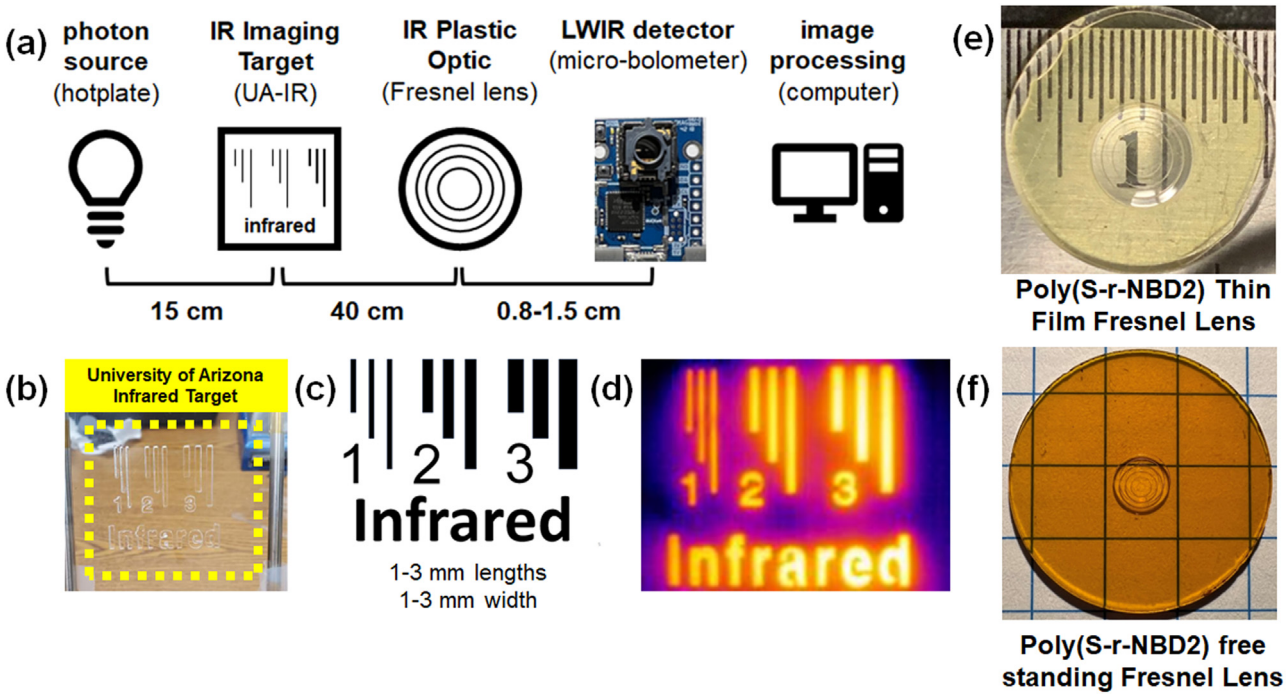

Fig. 9. (a) Schematic of labscale prototype LWIR imaging system; (b) UA-IR target fabricated for LWIR imaging standardization prepared from CO_2 laser writing into PMMA sheet; (c) specifications of UA-IR target pattern, with each line ranging from 1 to 3 mm in length and width; (d) representative LWIR image of UA-IR target; (e) poly(S-r-NBD2) with 50 wt% sulfur thin film Fresnel lens (0.1 mm, thick) cast onto a NaCl plate; and (f) poly(S-r-NBD2) with 50 wt% sulfur free standing Fresnel lens (1.0 mm, thick). Adapted with permission from[77], Copyright 2024 Wiley & Sons Publishing.

14 μm. With access to *CHIPs* Fresnel lenses and plano-convex Ge lenses possessing focal lengths of 13–14 mm, the entire LWIR system could be mounted on an air table, or even on laboratory bench tops, where laboratory scale hotplate-stirrers (or other blackbody radiators) could be used as an inexpensive IR photon source. To date, there still is no clear LWIR imaging protocol, or resolution targets to enable quanitative, uniform standardization of imaging experiments and new optical element optical characterization, as new LWIR imaging demonstrations are done with highly variable human subjects, or other macroscopic, commonplace tools, or objects (e.g., sodering irons, heating coils) [77].

In the fabrication of plastic optics, it is the ensemble of cost, optical/thermomechanical properties and polymer processabilty that determine suitability for final end-use as LWIR transmissive optical components. Poly(S-*r*-NBD2) (both 50-wt% and 70-wt% sulfur, referred to in this study as poly(S_{50}-*r*-NBD_{50}), or poly(S_{70}-*r*-DIB_{30}) Fresnel lenses were fabricated for imaging as these copolymers exhibited the most favorable synergy of properties (LWIR%T, glass transition (T_g)/thermal stability and melt processability). To fabricate these LWIR Fresnel plastics, a LWIR Fresnel lens master was designed in the LightTools simulation package and fabricated using diamond turning into a flat PMMA window (~4 mm thickness; 2 cm diameter), followed by replication in soft PDMS, which served as the mold for casting of sulfur copolymers. Both thin films (0.1 mm thick, supported on NaCl substrates)) and free standing (1.0 mm) Fresnel lenses from poly(S-*r*-NDB2) were fabricated to access the effect of film thickness and LWIR%T on LWIR imaging performance (Fig. 9e, f). First generation *CHIPs* based on poly(S-*r*-DIB) copolymers at the same composition (50-wt%, 70-wt% referred to as poly(S_{50}-*r*-DIB_{50}) and poly(S_{70}-*r*-DIB_{30})) were used as a control material reference for LWIR lenses of poly(S-*r*-NBD2) due to the observed inferior LWIR transparency/thermomechanical properties of poly(S-*r*-DIB), both of which were expected to compromise lens fabrication quality and imaging performance. LWIR experiments were initially conducted with a commercially available plano-convex singlet Ge lens (15 mm focal length, 5 mm thickness, with anti-reflective (AR) coating) from 100 to 30 °C (Fig. 10a), where sharp resolution of the UA-IR target was observed as expected across this full temperature range, with progressively reduced image brightness at lower temperatures due to lower IR photon flux generated from the blackbody radiator shown in Fig. 9b, c. It is important to note here that the AR-coating on the Ge lens significantly raised the LWIR transmission vs an uncoated Ge lens ($LWIR\%T_{with\ AR} > 90$ %T; $LWIR\%T_{without\ AR} > 50$ %T) and afforded higher resolution imaging at low temperatures [77].

LWIR imaging experiments on poly(S_{50}-*r*-$NBD2_{50}$) materials were initially done with supported thin film Fresnel lenses (peak thickness ~ 100 μm) cast onto NaCl substrates through the UA-IR PMMA target to ascertain both the true LWIR imaging quality and viable thermal imaging ranges of the intrinsic polymer material. The large form factor and limited manufacturabilty of NaCl plates frustrated direct integration of this lens architecture into LWIR imaging systems, as will be discussed in later sections. LWIR imaging over 100–30 °C was conducted (Fig. 10b), where excellent resolution and brightness was observed with the poly(S_{50}-*r*-$NBD2_{50}$) Fresnel lens from T = 100–60 °C. However, good resolution of the UA-IR target could still be achieved at T = 40–30 °C for only this particular Fresnel lens, with an accompanying reduction in image brightness, as observed for the AR-coated Ge lens reference. LWIR imaging with the higher sulfur content poly(S_{70}-*r*-$NBD2_{30}$) Fresnel lens was anticipated to afford better LWIR imaging and lower temperatures vs the 50-wt% copolymer experiments, due to the reduced content of the organic LWIR absorbing phase. While imaging of the UA-IR target is discernable from T = 100–60 °C with blurry imaging of the target at T = 40–30 °C (Fig. 10c), it is clear that these LWIR images have poor contrast in comparison to the results from the poly(S_{50}-*r*-$NBD2_{50}$) lens. This particular effect of LWIR imaging quality on sulfur copolymer compositions points to issues in the fabrication and quality of Fresnel lenses. The poly(S_{70}-*r*-$NBD2_{30}$), has both slightly lower T_g and more residual

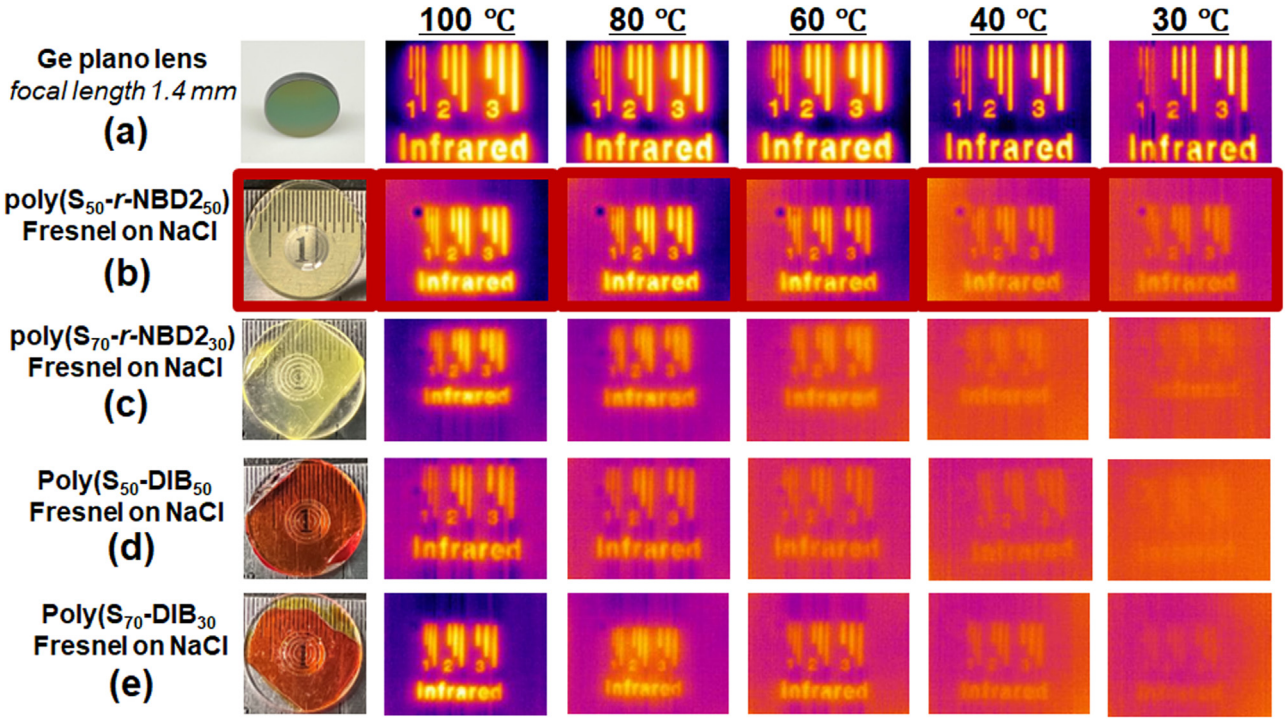

Fig. 10. Masked LWIR imaging experiments conducted with UA-IR target and labscale imaging system from Fig. 2 from T = 100–30 °C for: (a) 15 mm focal length plano-convex Ge lens as an imaging reference; (b) poly(S_{50}-r-$NBD2_{50}$); (c) poly(S_{70}-r-$NBD2_{30}$) thin film Fresnel lens on NaCl; (d) poly(S_{50}-r-DIB_{50}); and (e) poly(S_{70}-r-DIB_{30}) thin film Fresnel lens on NaCl. LWIR imaging was viable for poly(S_{50}-r-$NBD2_{50}$) Fresnel lens from T = 100–30 °C, while the control poly(S-r-DIB) Fresnel lenses possess inferior intrinsic LWIR transparency and was limited to imaging temperatures above T = 60 °C.). Adapted with permission from [77], Copyright 2024 Wiley & Sons Publishing.

unreacted S_8 in the glassy matrix of the lens, both of which may compromise the Fresnel lens quality (e.g., flatness, diffractive pattern resolution), increase scattering losses and present more challenges in optimizing the casting step into PDMS molds. Hence, the superior LWIR imaging quality achieved with the poly(S_{50}-*r*-$NBD2_{50}$) Fresnel lens reinforces the importance of both materials properties (optical, thermomechanical) and processability (castability, consumption of S_8 solid monomer) to achieve optimal imaging performance. LWIR imaging experiments with poly(S-*r*-DIB) Fresnel lenses of identical thickness supported on NaCl plates exhibited sigificantly smaller temperature ranges (T = 100–60 °C), where a significant reduction of LWIR imaging quality was observed below T = 60 °C for both 50-wt% and 70-wt% compositions (Fig. 10d, e). The reduced LWIR transmission of poly(S-*r*-DIB) vs poly(S-*r*-NBD2) is the most likely cause of poor LWIR imaging contrast in these experiments, although contributions from inferior thermomechanical properties and processability cannot be ruled out in this thin film NaCl supported lens architecture [77].

Access to these LWIR imaging experiments with consisent imaging targets and conditions enabled structure-property correlation for the first time of sulfur copolymer composition on LWIR lens performance. These measurements revealed that the highest contrast imaging was attained with the poly(S_{50}-*r*-$NBD2_{50}$) Fresnel lens with the poly(S_{70}-*r*-$NBD2_{30}$), poly(S_{50}-*r*-DIB_{50}) and poly(S_{70}-*r*-DIB_{30}) all exhibiting comparable levels of inferior imaging temperature ranges and resolution. An image resolution of 0.5 cycles/mm (since one cycle of lines is 2 mm) was esimated for the poly(S_{50}-*r*-$NBD2_{50}$) Fresnel lens images, based on the 1 mm thick lines in the UA-IR target; the image plane resolution being determined by the number of pixels from the dark point of the 1 mm line to the next dark or light side feature in the target. These experiments demonstrated the viabiltiy of using thin film sulfur copolymer IR lenses for LWIR imaging, particularly under ambient conditions. However, the need for NaCl supporting substrates prohibits integration into commerical IR imaging systems due to the moisture sensitivity and poor mechanical propeties of salt plates. Hence, much thicker freestanding Fresnel lens (thickness = 1.0 mm) fabricated via molding-casting were made from poly(S-r-NBD2) materials both at 50-wt% and 70-wt% sulfur compositions, along with poly(S-r-DIB) materials as the control. Both poly(S-*r*-NBD2) copolymer Frensel lenses possessed sufficient mechanical integrity to yield freestanding Frensel lenses of the target thickenss, however molded freestanding lenses from poly(S-r-DIB) were found to deform rapidly after mold release due to the low T_g of these sulfur copolymers. Both freestanding poly(S_{50}-*r*-$NBD2_{50}$) Fresnel lenses displayed comparable temperature ranges for discernible LWIR imaging of the UA-IR target (T = 200–60 °C), however, better resolution and focus was observed for the poly(S-*r*-NBD2) with 50 wt% sulfur, presumably due to the higher T_g and mechanical integrity of this plastic optic vs the same sulfur copolymer Fresnel lens made with 70-wt% sulfur. As anticipated, both freestanding poly(S-*r*-NBD2) Fresnel lenses required higher LWIR imaging temperatures to discern the UA-IR target and reduced imaging brightness vs the thin film poly(S-r-NBD2) Frensel lenses from Fig. 10. Furthermore, poly(S-*r*-DIB) freestanding Fresnel lens (thickness = 0.7 mm) exhibited the poorest imaging quality of the UA-IR target even at high temperature (T = 200 °C) in this series due to mechanical reflow from the low T_g coupled with the intrinsically low LWIR transmission of this material. These experiments clearly point to the need for both IR transpaency and thermomechanical properties to be jointly evaluated in new candidate sulfur polymeric materials for LWIR optics, as numerous new materials may possess improved IR transparency, but are usable for this application unless sufficiently glassy [77].

6. Conclusion and perspective

As discussed in this TREND, the development of high sulfur content polysulfides derived from the inverse vulcanization of elemental sulfur holds significant potential to broadly impact photonics and imaging systems across the infrared spectrum. The ad-

vances highlighted herein demonstrate the benefits of the high RI and high IR transparency of this novel class of optical polymers for a wide range of refractive optics and integrated photonic device constructs. While new advances in the design and synthesis of new inverse vulcanized polysulfides with improved thermomechanical and optical properties will certainly remain a critical effort to advance this field for IR optical applications, the development of novel polymer processing methods both in solution and in the melt will be required to fabricate new bulk and integrated optical components. The early work reported in this TREND clearly point to the viability of these new optical polymers and are anticipated to broadly impact the fields of polymer chemistry, petroleum science, commodity plastics and optical technologies.

Declaration of competing interest

The authors declare the following financial interests/personal relationships which may be considered as potential competing interests:

R. A. Norwood is an owner and officer of Norcon Technologies LLC with which a financial conflict of interest exists.

CRediT authorship contribution statement

Jeffrey Pyun: Writing – review & editing, Writing – original draft, Methodology, Investigation, Funding acquisition, Conceptualization. **Robert A. Norwood:** Writing – review & editing, Writing – original draft, Methodology, Investigation, Funding acquisition, Conceptualization.

Data availability

Data will be made available on request.

Acknowledgments

We gratefully acknowledge the National Science Foundation and the Air Force Research Laboratory through DMREF-2118578 for support of this work. The National Science Foundation (PFI-RP 1940942, MRI-1920234), the Air Force Research Laboratories (FA8650–16-D-5404), MOBASE, Hyundai Motor Company, the RII Research Advancement Grant program from the University of Arizona, the Arizona Technology and Research Initiative Fund (A.R.S.§15–1648) are also gratefully acknowledged. Gerald Uyeno and Raytheon Missiles Systems are gratefully acknowledged for helpful discussions and consultation on IR imaging system design.

Supplementary materials

Supplementary material associated with this article can be found, in the online version, at doi:10.1016/j.progpolymsci.2024.101865.

References

[1] Vollmer M, Möllmann KP. Fundamentals of infrared thermal imaging. Infrared Therm Imaging 2017:1–106. doi:10.1002/9783527693306.ch1.
[2] Kleine TS, Glass RS, Lichtenberger DL, Mackay ME, Char K, Norwood RA, et al. 100th anniversary of macromolecular science viewpoint: high refractive index polymers from elemental sulfur for infrared thermal imaging and optics. ACS Macro Lett 2020;9:245–59. doi:10.1021/acsmacrolett.9b00948.
[3] Eldada L, Shacklette LW. Advances in polymer integrated optics. IEEE J Sel Top Quantum Electron 2000;6:54–68. doi:10.1109/2944.826873.
[4] Ma H, Jen AKY, Dalton LR. Polymer-based optical waveguides: materials, processing, and devices. Adv Mater 2002;14:1339–65. doi: 10.1002/1521-4095(20021002)14:19⟨1339::AID-ADMA1339⟩3.0.CO;2-O.
[5] Dangel R, Horst F, Jubin D, Meier N, Weiss J, Offrein BJ, et al. Development of versatile polymer waveguide flex technology for use in optical interconnects. J Light Technol 2013;31:3915–26. doi:10.1109/JLT.2013.2282499.
[6] Kang JW, Kim JP, Lee WY, Kim JS, Lee JS, Kim JJ. Low-loss fluorinated poly(arylene ether sulfide) waveguides with high thermal stability. J Light Technol 2001;19:872–5. doi:10.1109/50.927521.
[7] Lindenmann N, Balthasar G, Hillerkuss D, Schmogrow R, Jordan M, Leuthold J, et al. Photonic wire bonding: a novel concept for chip-scale interconnects. Opt Express 2012;20:17667. doi:10.1364/oe.20.017667.
[8] Rezem M, Gunther A, Roth B, Reithmeier E, Rahlves M. Low-cost fabrication of all-polymer components for integrated photonics. J Light Technol 2017;35:299–308. doi:10.1109/JLT.2016.2639740.
[9] Yasuhara K, Yu F, Ishigure T. Circular core single-mode polymer optical waveguide fabricated using the Mosquito method with low loss at 1310/1550 nm. Opt Express 2017;25:8524. doi:10.1364/oe.25.008524.
[10] Zuo H, Yu S, Gu T, Hu J. Low loss, flexible single-mode polymer photonics. Opt Express 2019;27:11152. doi:10.1364/oe.27.011152.
[11] Anderson LE, Kleine TS, Zhang Y, Phan DD, Namnabat S, LaVilla EA, et al. Chalcogenide hybrid inorganic/organic polymers: ultrahigh refractive index polymers for infrared imaging. ACS Macro Lett 2017;6:500–4. doi:10.1021/acsmacrolett.7b00225.
[12] Babaeian M, Diaz LR, Namnabat S, Kleine TS, Azarm A, Pyun J, et al. Nonlinear optical properties of chalcogenide hybrid inorganic/organic polymers (CHIPs) using the Z-scan technique. Opt Mater Express 2018;8:2510. doi:10.1364/ome.8.002510.
[13] Griebel JJ, Namnabat S, Kim ET, Himmelhuber R, Moronta DH, Chung WJ, et al. New infrared transmitting material via inverse vulcanization of elemental sulfur to prepare high refractive index polymers. Adv Mater 2014;26:3014–18. doi:10.1002/adma.201305607.
[14] Griebel JJ, Nguyen NA, Namnabat S, Anderson LE, Glass RS, Norwood RA, et al. Dynamic covalent polymers via inverse vulcanization of elemental sulfur for healable infrared optical materials. ACS Macro Lett 2015;4:862–6. doi:10.1021/acsmacrolett.5b00502.
[15] Kleine TS, Diaz LR, Konopka KM, Anderson LE, Pavlopolous NG, Lyons NP, et al. One dimensional photonic crystals using ultrahigh refractive index chalcogenide hybrid inorganic/organic polymers. ACS Macro Lett 2018;7:875–80. doi:10.1021/acsmacrolett.8b00245.
[16] Kleine TS, Lee T, Carothers KJ, Hamilton MO, Anderson LE, Ruiz Diaz L, et al. Infrared fingerprint engineering: a molecular-design approach to long-wave infrared transparency with polymeric materials. Angew Chem Int Ed 2019;58:17656–60. doi:10.1002/anie.201910856.
[17] Kleine TS, Nguyen NA, Anderson LE, Namnabat S, LaVilla EA, Showghi SA, et al. High Refractive index copolymers with improved thermomechanical properties via the inverse vulcanization of sulfur and 1,3,5-triisopropenylbenzene. ACS Macro Lett 2016;5:1152–6. doi:10.1021/acsmacrolett.6b00602.
[18] Chung WJ, Griebel JJ, Kim ET, Yoon H, Simmonds AG, Ji HJ, et al. The use of elemental sulfur as an alternative feedstock for polymeric materials. Nature Chem 2013;5:518–24. doi:10.1038/nchem.1624.
[19] Lim J, Pyun J, Char K. Recent approaches for the direct use of elemental sulfur in the synthesis and processing of advanced materials. Angew Chem Int Ed 2015;54:3249–58. doi:10.1002/anie.201409468.
[20] Griebel JJ, Glass RS, Char K, Pyun J. Polymerizations with elemental sulfur: a novel route to high sulfur content polymers for sustainability, energy and defense. Prog Polym Sci 2016;58:90–125. doi:10.1016/j.progpolymsci.2016.04.003.
[21] Worthington MJH, Kucera RL, Chalker JM. Green chemistry and polymers made from sulfur. Green Chem 2017;19:2748–61. doi:10.1039/C7GC00014F.
[22] Chalker JM, Worthington MJH, Lundquist NA, Esdaile LJ. Synthesis and applications of polymers made by inverse vulcanization. Top Curr Chem 2019;377:16. doi:10.1007/s41061-019-0242-7.
[23] Zhang Y, Glass RS, Char K, Pyun J. Recent advances in the polymerization of elemental sulphur, inverse vulcanization and methods to obtain functional chalcogenide hybrid inorganic/organic polymers (CHIPs). Polym Chem 2019;10:4078–105. doi:10.1039/C9PY00636B.
[24] Lee T, Dirlam PT, Njardarson JT, Glass RS, Pyun J. Polymerizations with elemental sulfur: from petroleum refining to polymeric materials. JACS 2022;144:5–22. doi:10.1021/jacs.1c09329.
[25] Jang W, Choi K, Choi JS, Kim DH, Char K, Lim J, et al. Transparent, ultrahigh-refractive index polymer film (n ~1.97) with minimal birefringence (Δn <0.0010). ACS Appl Mater Interfaces 2021;13:61629–37. doi:10.1021/acsami.1c17398.
[26] Jang W, Choi K, Kang M, Park S, Kim DH, Ahn J, et al. Visible, mid- and long-wave infrared transparent sulfur-rich polymer with enhanced thermal stability. Chem Mater 2023;35:8181–91. doi:10.1021/acs.chemmater.3c01679.
[27] Kim DH, Jang W, Choi K, Choi JS, Pyun J, Lim J, et al. One-step vapor-phase synthesis of transparent high refractive index sulfur-containing polymers. Sci Adv 2020;6:eabb5320. https://www.science.org/doi/abs/10.1126/sciadv.abb5320.
[28] Ye P, Hong Z, Loy DA, Liang R. UV-curable thiol-ene system for broadband infrared transparent objects. Nat Commun 2023;14:8385. doi:10.1038/s41467-023-44273-0.
[29] Bao J, Martin KP, Cho E, Kang KS, Glass RS, Coropceanu V, et al. On the mechanism of the inverse vulcanization of elemental sulfur: structural characterization of poly(sulfur-random-(1,3-diisopropenylbenzene)). JACS 2023;145:12386–97. doi:10.1021/jacs.3c03604.
[30] Qureshi MH, Bao J, Kleine TS, Kim KJ, Carothers KJ, Molineux J, et al. Synthesis of deuterated and sulfurated polymers by inverse vulcanization: engineering infrared transparency via deuteration. JACS 2023;145:27821–9. doi:10.1021/jacs.3c10985.

[31] Nishant A, Kim KJ, Showghi SA, Himmelhuber R, Kleine TS, Lee T, et al. High refractive index chalcogenide hybrid inorganic/organic polymers for integrated photonics. Adv Opt Mater 2022;10:2200176. doi:10.1002/adom.202200176.
[32] Bischoff DJ, Lee T, Kang KS, Molineux J, O'Neil Parker W, Pyun J, et al. Unraveling the rheology of inverse vulcanized polymers. Nat Commun 2023;14:7553. doi:10.1038/s41467-023-43117-1.
[33] Park S, Lee D, Cho H, Lim J, Char K. Inverse vulcanization polymers with enhanced thermal properties via divinylbenzene homopolymerization-assisted cross-linking. ACS Macro Lett 2019;8:1670–5. doi:10.1021/acsmacrolett.9b00827.
[34] Orme K, Fistrovich AH, Jenkins CL. Tailoring polysulfide properties through variations of inverse vulcanization. Macromolecules 2020;53:9353–61. doi:10.1021/acs.macromol.0c01932.
[35] Choi K, Jang W, Lee W, Choi JS, Kang M, Kim J, et al. Systematic control of sulfur chain length of high refractive index, transparent sulfur-containing polymers with enhanced thermal stability. Macromolecules 2022;55:7222–31. doi:10.1021/acs.macromol.2c00537.
[36] He L, Yang J, Jiang H, Zhao H, Xia H. Mechanochemistry enabled inverse vulcanization of norbornadiene for optical polymers and elastomeric materials. Ind Eng Chem Res 2023;62:9587–94. doi:10.1021/acs.iecr.3c00801.
[37] Tonkin SJ, Pham LN, Gascooke JR, Johnston MR, Coote ML, Gibson CT, et al. Thermal imaging and clandestine surveillance using low-cost polymers with long-wave infrared transparency. Adv Opt Mater 2023;11:2300058. doi:10.1002/adom.202300058.
[38] Arouh S, Nishant A, Pyun J, Norwood RA. Characterization of the optical and electronic properties of chalcogenide hybrid inorganic/organic polymer thin films. Opt Mater Express 2023;13:2737–45. doi:10.1364/OME.499063.
[39] Sieger M, Mizaikoff B. Toward on-chip mid-infrared sensors. Anal Chem 2016;88:5562–73. doi:10.1021/acs.analchem.5b04143.
[40] Yoo KM, Midkiff J, Rostamian A, Chung C-j, Dalir H, Chen RT. InGaAs membrane waveguide: a promising platform for monolithic integrated mid-infrared optical gas sensor. ACS Sens 2020;5:861–9. doi:10.1021/acssensors.0c00180.
[41] Grotevent MJ, Yakunin S, Bachmann D, Romero C, Vázquez de Aldana JR, Madi M, et al. Integrated photodetectors for compact Fourier-transform waveguide spectrometers. Nat Photonics 2023;17:59–64. doi:10.1038/s41566-022-01088-7.
[42] Edrington AC, Urbas AM, DeRege P, Chen CX, Swager TM, Hadjichristidis N, et al. Polymer-based photonic crystals. Adv Mater 2001;13:421–5. doi: 10.1002/1521-4095(200103)13:6⟨421::AID-ADMA421⟩3.0.CO;2-#.
[43] Park C, Yoon J, Thomas EL. Enabling nanotechnology with self assembled block copolymer patterns. Polymer 2003;44:6725–60 (Guildf). doi:10.1016/j.polymer.2003.08.011.
[44] Sveinbjörnsson BR, Weitekamp RA, Miyake GM, Xia Y, Atwater HA, Grubbs RH. Rapid self-assembly of brush block copolymers to photonic crystals. PNAS 2012;109:14332. doi:10.1073/pnas.1213055109.
[45] Lova P, Manfredi G, Comoretto D. Advances in functional solution processed planar 1D photonic crystals. Adv Opt Mater 2018;6:1800730. doi:10.1002/adom.201800730.
[46] Shneidman AV, Becker KP, Lukas MA, Torgerson N, Wang C, Reshef O, et al. All-polymer integrated optical resonators by roll-to-roll nanoimprint lithography. ACS Photonics 2018;5:1839–45. doi:10.1021/acsphotonics.8b00022.
[47] Tavella C, Lova P, Marsotto M, Luciano G, Patrini M, Stagnaro P, et al. High refractive index inverse vulcanized polymers for organic photonic crystals. Crystals 2020;10:154. (Basel) https://www.mdpi.com/2073-4352/10/3/154 .
[48] Tsay C, Toor F, Gmachl CF, Arnold CB. Chalcogenide glass waveguides integrated with quantum cascade lasers for on-chip mid-IR photonic circuits. Opt Lett 2010;35:3324. doi:10.1364/OL.35.003324.
[49] Xia X, Chen Q, Tsay C, Arnold CB, Madsen CK. Low-loss chalcogenide waveguides on lithium niobate for the mid-infrared. Opt Lett 2010;35:3228. doi:10.1364/OL.35.003228.
[50] Zou Y, Moreel L, Lin H, Zhou J, Li L, Danto S, et al. Solution processing and resist-free nanoimprint fabrication of thin film chalcogenide glass devices: inorganic-organic hybrid photonic integration. Adv Opt Mater 2014;2:759–64. doi:10.1002/adom.201400068.
[51] Dangel R, Hofrichter J, Horst F, Jubin D, La Porta A, Meier N, et al. Polymer waveguides for electro-optical integration in data centers and high-performance computers. Opt Express 2015;23:4736. doi:10.1364/oe.23.004736.
[52] Morarescu R, Pal PK, Beneitez NT, Missinne J, Steenberge GV, Bienstman P, et al. Fabrication and characterization of high-optical-quality-factor hybrid polymer microring resonators operating at very near infrared wavelengths. IEEE Photonics J 2016;8:1–9. doi:10.1109/JPHOT.2016.2544641.
[53] Gurton KP, Yuffa AJ, Videen GW. Enhanced facial recognition for thermal imagery using polarimetric imaging. Opt Lett 2014;39:3857–9. doi:10.1364/OL.39.003857.
[54] Hwang J, Oh B, Kim Y, Silva S, Kim JO, Czaplewski DA, et al. Fabry-Perot cavity resonance enabling highly polarization-sensitive double-layer gold grating. Sci Rep 2018;8:14787. doi:10.1038/s41598-018-32158-y.
[55] Sanghera JS, Shaw LB, Aggarwal ID. Applications of chalcogenide glass optical fibers. C R Chim 2002;5:873–83. doi:10.1016/s1631-0748(02)01450-9.
[56] Islam MD, Kim JO, Ko Y, Ku Z, Boyd DA, Smith EM, et al. Design of high efficient mid-wavelength infrared polarizer on ormochalc polymer. Macromol Mater Eng 2020;305:2000033. doi:10.1002/mame.202000033.
[57] Berndt AJ, Hwang J, Islam MD, Sihn A, Urbas AM, Ku Z, et al. Poly(sulfur-random-(1,3-diisopropenylbenzene)) based mid-wavelength infrared polarizer: optical property experimental and theoretical analysis. Polymer 2019;176:118–26 (Guildf). doi:10.1016/j.polymer.2019.05.036.
[58] Cho W, Hwang J, Lee SY, Park J, Han N, Lee CH, et al. Highly sensitive and cost-effective polymeric-sulfur-based mid-wavelength infrared linear polarizers with tailored fabry–pérot resonance. Adv Mater 2023;35:2209377. doi:10.1002/adma.202209377.
[59] Gou F, Peng F, Ru Q, Lee YH, Chen H, He Z, et al. Mid-wave infrared beam steering based on high-efficiency liquid crystal diffractive waveplates. Opt Express 2017;25:22404–10. doi:10.1364/OE.25.022404.
[60] Zou Y, Chakravarty S, Chung CJ, Xu X, Chen RT. Mid-infrared silicon photonic waveguides and devices. Photon Res 2018;6:254–76. doi:10.1364/PRJ.6.000254.
[61] Yadav A, Agarwal AM. Integrated photonic materials for the mid-infrared. Int J Appl Glass Sci 2020;11:491–510. doi:10.1111/ijag.15252.
[62] Farrell WS, Orski SV, Kotula AP, Baugh Iii DW, Snyder CR, Beers KL. Precision, tunable deuterated polyethylene via polyhomologation. Macromolecules 2019;52:5741–9. doi:10.1021/acs.macromol.9b00500.
[63] Li L, Jakowski J, Do C, Hong K. Deuteration and polymers: rich history with great potential. Macromolecules 2021;54:3555–84. doi:10.1021/acs.macromol.0c02284.
[64] Dislich H. Plastics as optical materials. Angew Chem Int Ed 1979;18:49–59. doi:10.1002/anie.197900491.
[65] Chandrinos A. High refractive index plastic optical materials. Saarbrucken: VDM Verlag; 2009.
[66] Sussman M. Elementary diffraction theory of zone plates. Am J Phys 1960;28:394–8. doi:10.1119/1.1935811.
[67] Engelberg J, Levy U. The advantages of metalenses over diffractive lenses. Nature Commun 2020;11:1991. doi:10.1038/s41467-020-15972-9.
[68] Chen MK, Wu Y, Feng L, Fan Q, Lu M, Xu T, et al. Principles, functions, and applications of optical meta-lens. Adv Opt Mater 2021;9:2001414. doi:10.1002/adom.202001414.
[69] Meem M, Banerji S, Majumder A, Vasquez FG, Sensale-Rodriguez B, Menon R. Broadband lightweight flat lenses for long-wave infrared imaging. PNAS 2019;116:21375–8. doi:10.1073/pnas.1908447116.
[70] Manaf ARA, Sugiyama T, Yan J. Design and fabrication of Si-HDPE hybrid Fresnel lenses for infrared imaging systems. Opt Express 2017;25:1202–20. doi:10.1364/OE.25.001202.
[71] Bradburn G. Design and manufacture of high quality plastic infrared fresnel lenses: Proc spie 0590, infrared technology and applications, 1986. 10.1117/12.951969
[72] Boyd DA, Nguyen VQ, McClain CC, Kung FH, Baker CC, Myers JD, et al. Optical properties of a sulfur-rich organically modified chalcogenide polymer synthesized via inverse vulcanization and containing an organometallic comonomer. ACS Macro Lett 2019;8:113–16. doi:10.1021/acsmacrolett.8b00923.
[73] Lee JM, Noh GY, Kim BG, Yoo Y, Choi WJ, Kim DG, et al. Synthesis of poly(phenylene polysulfide) networks from elemental sulfur and p-diiodobenzene for stretchable, healable, and reprocessable infrared optical applications. ACS Macro Lett 2019;8:912–16. doi:10.1021/acsmacrolett.9b00306.
[74] Lee M, Oh Y, Yu J, Jang SG, Yeo H, Park JJ, et al. Long-wave infrared transparent sulfur polymers enabled by symmetric thiol cross-linker. Nature Commun 2023;14:2866. doi:10.1038/s41467-023-38398-5.
[75] Hwang JH, Kim SH, Cho W, Lee W, Park S, Kim YS, et al. A Microphase separation strategy for the infrared transparency-thermomechanical property conundrum in sulfur-rich copolymers. Adv Opt Mater 2023;11:2202432. https://onlinelibrary.wiley.com/doi/abs/10.1002/adom.202202432.
[76] Jeon Y, Choi J, Seo D, Jung SH, Lim J. Low birefringence and low dispersion aliphatic thermosets with a high and tunable refractive index. Polym Chem 2023;14:1117–23. doi:10.1039/D2PY01327D.
[77] Molineux J, Lee T, Kim KJ, Kang KS, Lyons NP, Nishant A, et al. Fabrication of plastic optics from chalcogenide hybrid inorganic/organic polymers for infrared thermal imaging. Adv Opt Mater 2024;12:2301971. https://onlinelibrary.wiley.com/doi/abs/10.1002/adom.202301971.